CERN–TH/96–119
LU TP 96–13
May 1996

A scenario for high-energy $\gamma\gamma$ interactions

Gerhard A. Schuler[a]

Theory Division, CERN,
CH-1211 Geneva 23, Switzerland
E-mail: schulerg@cernvm.cern.ch

and

Torbjörn Sjöstrand

Department of Theoretical Physics,
University of Lund, Lund, Sweden
E-mail: torbjorn@thep.lu.se

Abstract

A real photon has a complicated nature, whereby it may remain unresolved or fluctuate into a vector meson or a perturbative $q\overline{q}$ pair. In $\gamma\gamma$ events, this gives three by three combinations of the nature of the two incoming photons, and thus six distinct event classes. The properties of these classes are partly constrained by the choices already made in our related γp model. It is therefore possible to predict the energy-dependence of the cross section for each of the six components separately. The total cross section gives support to the idea that a simple factorized ansatz with a pomeron and a reggeon term can be a good approximation. Event properties undergo a stepwise evolution from pp to γp to $\gamma\gamma$ events, with larger charged multiplicity, more transverse energy flow and a higher jet rate in the latter process.

---

[a] Heisenberg Fellow.

1 Introduction

There are many reasons for being interested in $\gamma\gamma$ physics. The collision between two photons provides the richest spectrum of (leading-order) processes that is available for any choice of two incoming elementary particles. For instance, since the photon has a hadronic component, all of hadronic physics is contained as a subset of the possibilities. Additionally, the photon can appear as an unresolved particle or as a perturbative $\mathrm{q\overline{q}}$ fluctuation, giving a host of possible further interaction processes. The relative amount of these components and their respective properties are not fully understood today. A correct description of the components of the total $\gamma\gamma$ cross section and the related event shapes therefore is the ultimate challenge of 'minimum-bias' physics. Specific issues include the description of the photon wave function, duality between perturbative and nonperturbative descriptions of the resolved photon, the rôle of multiple parton–parton interactions and the related minijet phenomenology and eikonalization of the total cross section, the transition between soft and hard physics, the transition between the real photon and the virtual one, and so on.

In addition to the direct reasons, there are also indirect ones. The process $\mathrm{e^+e^-} \to \mathrm{e^+e^-}\gamma\gamma \to \mathrm{e^+e^-}X$ will be a main one at LEP 2 and future linear $\mathrm{e^+e^-}$ colliders. Therefore, $\gamma\gamma$ events are always going to give a non-negligible background to whatever other physics one is interested in. The devising of efficient analysis strategies must be based on a good understanding of $\gamma\gamma$ physics.

The study of $\gamma\gamma$ physics has a long history, and it is not our intention here to give a complete list of references. Many topics have been covered by contributions to past workshops [1]. In recent years HERA has been providing rich information on the related $\gamma\mathrm{p}$ processes, and thereby stimulating the whole field [2]. Further developments can be expected here. Currently $\gamma\gamma$ interest is focussed on LEP 2 [3]. Already LEP 1.5 has provided ample reminder of the important rôle of $\gamma\gamma$ processes when away from the $\mathrm{Z^0}$ pole. LEP 2 brings the promise of a large event rate at reasonably large $\gamma\gamma$ energies. In the future, the laser backscattering option of linear $\mathrm{e^+e^-}$ colliders offers the promise of obtaining a large rate of very high-energy $\gamma\gamma$ interactions, typically at up to 70% of the energy of the corresponding $\mathrm{e^+e^-}$ collisions. Then the two aspects above come together in force, both with new chances to understand photon interactions and new challenges to eliminate the $\gamma\gamma$ background to other processes.

The starting point for the current paper is our model for $\gamma\mathrm{p}$ physics [4]. Many of the basic assumptions can be taken over in an (almost) minimal fashion, while further new ones appear. Based on the experience from HERA, some old assumptions can be sharpened and further developed. LEP 2 and future linear colliders will allow new tests to be carried out. Our recent studies on the parton distributions of the photon [5] are parts of the same physics program, and provide further important building blocks for the current study. In this paper we also emphasize the gradual evolution from pp to $\gamma\mathrm{p}$ to $\gamma\gamma$ events, that allows some cross-checks to be carried out systematically. Parts of this work has already been presented in a preliminary form at workshops [6, 7].

No model exists in a vacuum. For the approach we are going to take, one important line of work is the subdivision of photon interactions by the nature of the photon [8]. Minijet phenomenology has attracted much attention in recent years [9]. Other related works will appear as we go along. However, none of these approaches attempts to give a complete description of $\gamma\gamma$ cross sections and event properties, but only concentrate on specific topics. Here we will try to be more ambitious, and really provide all the necessary

aspects in one single framework. The only other work with a somewhat similar global scope is the recent studies within the context of dual topological unitarization [10].

Some main areas are still left out of our description. In all that follows, both incoming photons are assumed to be on the mass shell; further issues need to be addressed when either photon or both of them are virtual. The issue of the eikonalization of the anomalous and direct components of the photon wave function will be partly deferred to future studies; the evidence for some form of eikonalization will become apparent as we go along. Finally, for reasons of clarity, we restrict ourselves to discussing what happens in the collision between two photons of given momenta. The addition of photon flux factors [3] complicates the picture, but does not add anything fundamentally new.

Section 2 contains a description of the photon wave function and $\gamma\gamma$ event classes, section 3 of total and partial cross sections, section 4 of event properties and section 5 gives a summary and outlook.

2 The Photon Wave Function and Event Classes

To first approximation, the photon is a point-like particle. However, quantum mechanically, it may fluctuate into a (charged) fermion–antifermion pair. The fluctuations $\gamma \leftrightarrow \mathrm{q\overline{q}}$ are of special interest to us, since such fluctuations can interact strongly and therefore turn out to be responsible for the major part of the γp and $\gamma\gamma$ total cross sections, as we shall see. On the other hand, the fluctuations into a lepton pair are uninteresting, since such states do not undergo strong interactions to leading order, and therefore contribute negligibly to total hadronic cross sections. The leptonic fluctuations are perturbatively calculable, with an infrared cut-off provided by the lepton mass itself. Not so for quark pairs, where low-virtuality fluctuations enter a domain of non-perturbative QCD physics. It is therefore customary to split the spectrum of fluctuations into a low-virtuality and a high-virtuality part. The former part can be approximated by a sum over low-mass vector-meson states, customarily (but not necessarily) restricted to the lowest-lying vector multiplet. Phenomenologically, this Vector Meson Dominance (VMD) ansatz turns out to be very successful in describing a host of data. The high-virtuality part, on the other hand, should be in a perturbatively calculable domain.

In total, the photon wave function can then be written as [4]

$$|\gamma\rangle = c_{\mathrm{bare}}|\gamma_{\mathrm{bare}}\rangle + \sum_{V=\rho^0,\omega,\phi,\mathrm{J}/\psi} c_V|V\rangle + \sum_{\mathrm{q=u,d,s,c,b}} c_{\mathrm{q}}|\mathrm{q\overline{q}}\rangle + \sum_{\ell=\mathrm{e},\mu,\tau} c_\ell|\ell^+\ell^-\rangle \qquad (1)$$

(neglecting the small contribution from Υ). In general, the coefficients c_i depend on the scale μ used to probe the photon. Thus $c_\ell^2 \approx (\alpha_{\mathrm{em}}/2\pi)(2/3)\ln(\mu^2/m_\ell^2)$. Introducing a cut-off parameter k_0 to separate the low- and high-virtuality parts of the $\mathrm{q\overline{q}}$ fluctuations, one similarly obtains $c_{\mathrm{q}}^2 \approx (\alpha_{\mathrm{em}}/2\pi)2e_{\mathrm{q}}^2\ln(\mu^2/k_0^2)$. Since each $\mathrm{q\overline{q}}$ fluctuation is characterized by some virtuality or transverse momentum scale k, the notation in eq. (1) should really be viewed as shorthand, where the full expression is obtained by

$$c_{\mathrm{q}}|\mathrm{q\overline{q}}\rangle \longmapsto \frac{\alpha_{\mathrm{em}}}{2\pi}\,2e_{\mathrm{q}}^2\int_{k_0^2}^{\mu^2}\frac{\mathrm{d}k^2}{k^2}\,|\mathrm{q\overline{q}};k^2\rangle\ , \qquad (2)$$

and correspondingly for the lepton component. This is the form assumed in the following. The VMD part corresponds to the range of $\mathrm{q\overline{q}}$ fluctuations below k_0 and is thus μ-independent (assuming $\mu > k_0$). In conventional notation $c_V^2 = 4\pi\alpha_{\mathrm{em}}/f_V^2$, with $f_V^2/4\pi$

determined from data to be 2.20 for ρ^0, 23.6 for ω, 18.4 for ϕ and 11.5 for J/ψ [11]. Finally, $c_{\rm bare}$ is given by unitarity: $c^2_{\rm bare} \equiv Z_3 = 1 - \sum c_V^2 - \sum c_{\rm q}^2 - \sum c_\ell^2$. In practice, $c_{\rm bare}$ is always close to unity. Usually the probing scale μ is taken to be the transverse momentum of a $2 \to 2$ parton-level process. Our fitted value $k_0 \approx 0.5$ GeV [4] then sets the minimum transverse momentum of a perturbative branching $\gamma \to {\rm q}\overline{\rm q}$.

In part, k_0 is an unphysical parameter, and one would expect a continuity under reasonably variations of it. That is, if the VMD sum were to be extended beyond the lowest-lying vector mesons to also include higher resonances, it should be possible to compensate this by using a correspondingly higher k_0 cut-off for the continuous perturbative spectrum. This may provide some guidelines when exploring the physics implications of the ansatz above. The VMD–perturbative state duality has its limits, however. Higher excitations of vector mesons have larger wave-function radii than the lowest-lying states when each is produced 'on shell' in the time-like region (roughly $r \propto m$), while the uncertainty relation gives smaller radii for the higher-virtuality components of the real photon wave function ($r \propto 1/m$). Correspondingly, the contributions of ρ^0, ω and ϕ could not well be described by perturbation theory alone: the c_V parameters are related to the absolute rates of the elastic processes $\gamma{\rm p} \to V{\rm p}$, and here the observed relation between ρ^0 and ω production is in agreement with the 9 : 1 VMD expectations of coherent vector meson wave-functions, while incoherent interactions of perturbative components $|{\rm u}\overline{\rm u}\rangle$ and $|{\rm d}\overline{\rm d}\rangle$ would have lead to equal production of ρ^0 and ω.

The subdivision of the above photon wave function corresponds to the existence of three main event classes in γp events, cf. Fig. 1:

1. The VMD processes, where the photon turns into a vector meson before the interaction, and therefore all processes allowed in hadronic physics may occur. This includes elastic and diffractive scattering as well as low-$p_\perp$ and high-$p_\perp$ non-diffractive events.
2. The direct processes, where a bare photon interacts with a parton from the proton.
3. The anomalous processes, where the photon perturbatively branches into a $\rm q\overline{q}$ pair, and one of these (or a daughter parton thereof) interacts with a parton from the proton.

All three processes are of $O(\alpha_{\rm em})$. However, in the direct contribution the 'parton' distribution of the photon is of $O(1)$ and the hard scattering matrix elements of $O(\alpha_{\rm em})$, while the opposite holds for the VMD and the anomalous processes. As we already noted, the $\ell^+\ell^-$ fluctuations are not interesting, and there is thus no class associated with them.

The above subdivision is not unique, or even the conventional one. More common is to lump the jet production processes of VMD and anomalous into a class called resolved photons. The remaining 'soft-VMD' class is then defined as not having any jet production at all, but only consisting of low-$p_\perp$ events. We find such a subdivision counterproductive, since it is then not possible to think of the VMD class as being a scaled-down version (by a factor c_V^2) of ordinary hadronic processes — remember that normal hadronic collisions *do* contain jets part of the time.

In a complete framework, there would be no sharp borders between the three above classes, but rather fairly smooth transition regions that interpolate between the extreme behaviours. However, at our current level of understanding, we do not know how to do this, and therefore push our ignorance into parameters such as the k_0 scale and the $f_V^2/4\pi$ couplings. From a practical point of view, the sharp borders on the parton level are smeared out by parton showers and hadronization. Any Monte Carlo event sample intended to catch a border region would actually consist of a mixture of the three ex-

treme scenarios, and therefore indeed be intermediate. This issue is discussed further in section 3.3.

The difference between the three classes is easily seen in terms of the beam jet structure. The incoming proton always gives a beam jet containing the partons of the proton that did not interact. On the photon side, the direct processes do not give a beam jet at all, since all the energy of the photon is involved in the hard interaction. The VMD ones (leaving aside the elastic and diffractive subprocesses for the moment) give a beam remnant just like the proton, with a 'primordial $k_\perp$' smearing of typically up to half a GeV. The anomalous processes give a beam remnant produced by the $\gamma \to \mathrm{q}\overline{\mathrm{q}}$ branching, with a transverse momentum going from k_0 upwards. Thus the transition from VMD to anomalous should be rather smooth.

A generalization of the above picture to $\gamma\gamma$ events is obtained by noting that each of the two incoming photons is described by a wave function of the type given in eq. (1). In total, there are therefore three times three event classes. By symmetry, the 'off-diagonal' combinations appear pairwise, so the number of distinct classes is only six. These are, cf. Fig. 2:

1. VMD$\times$VMD: both photons turn into hadrons, and the processes are therefore the same as allowed in hadron–hadron collisions.
2. VMD$\times$direct: a bare photon interacts with the partons of the VMD photon.
3. VMD$\times$anomalous: the anomalous photon perturbatively branches into a $\mathrm{q}\overline{\mathrm{q}}$ pair, and one of these (or a daughter parton thereof) interacts with a parton from the VMD photon.
4. Direct$\times$direct: the two photons directly give a quark pair, $\gamma\gamma \to \mathrm{q}\overline{\mathrm{q}}$. Also lepton pair production is allowed, $\gamma\gamma \to \ell^+\ell^-$, but will not be considered by us.
5. Direct$\times$anomalous: the anomalous photon perturbatively branches into a $\mathrm{q}\overline{\mathrm{q}}$ pair, and one of these (or a daughter parton thereof) directly interacts with the other photon.
6. Anomalous$\times$anomalous: both photons perturbatively branch into $\mathrm{q}\overline{\mathrm{q}}$ pairs, and subsequently one parton from each photon undergoes a hard interaction.

The first three classes above are pretty much the same as the three classes allowed in γp events, since the interactions of a VMD photon and those of a proton are about the same.

The main parton-level processes that occur in the six classes are:

- The 'direct' processes $\gamma\gamma \to \mathrm{q}\overline{\mathrm{q}}$ only occur in class 4.
- The '1-resolved' processes $\gamma\mathrm{q} \to \mathrm{qg}$ and $\gamma\mathrm{g} \to \mathrm{q}\overline{\mathrm{q}}$ occur in classes 2 and 5.
- The '2-resolved' processes $\mathrm{qq}' \to \mathrm{qq}'$ (where q' may also represent an antiquark), $\mathrm{q}\overline{\mathrm{q}} \to \mathrm{q}'\overline{\mathrm{q}}'$, $\mathrm{q}\overline{\mathrm{q}} \to \mathrm{gg}$, $\mathrm{qg} \to \mathrm{qg}$, $\mathrm{gg} \to \mathrm{q}\overline{\mathrm{q}}$ and $\mathrm{gg} \to \mathrm{gg}$ occur in classes 1, 3 and 6.
- Elastic, diffractive and low-$p_\perp$ events occur in class 1.

In the list above we have only indicated the lowest-order processes. Within the context of the leading-log approximation, at least, the subdivision into six event classes is easily generalized to graphs with an arbitrary number of partons in the final state. This classification is illustrated in Fig. 3 for a generic ladder graph. To this picture final-state radiation can be added trivially.

The notation direct, 1-resolved and 2-resolved is the conventional subdivision of $\gamma\gamma$ interactions. The rest is then called 'soft-VMD'. As for the γp case, our subdivision is an attempt to be more precise and internally consistent than the conventional classes allow. One aspect is that we really want to have a VMD$\times$VMD class that is nothing but a scaled-down copy of the $\rho^0\rho^0$ and other vector-meson processes, with a consistent

transition between low-$p_\perp$ and high-$p_\perp$ events (see below). Another aspect is that, in a complete description, the VMD and anomalous parts of the photon give rise to different beam remnant structures, as discussed above, even when the hard subprocess itself may be the same.

A third aspect is that our subdivision provides further constraints; these, at least in principle, make the model more predictive. In particular, the parton distributions of the photon are constrained by the ansatz in eq. (1) to be given by

$$f_a^\gamma(x,\mu^2) = f_a^{\gamma,\mathrm{dir}}(x,\mu^2) + f_a^{\gamma,\mathrm{VMD}}(x,\mu^2) + f_a^{\gamma,\mathrm{anom}}(x,\mu^2;k_0^2) \; . \tag{3}$$

Here

$$f_a^{\gamma,\mathrm{dir}}(x,\mu^2) = Z_3 \, \delta_{a\gamma} \, \delta(1-x) \tag{4}$$

and

$$f_a^{\gamma,\mathrm{VMD}}(x,\mu^2) = \sum_{V=\rho^0,\omega,\phi,\mathrm{J}/\psi} \frac{4\pi\alpha}{f_V^2} f_a^V(x,\mu^2) \; . \tag{5}$$

The anomalous part, finally, is fully calculable perturbatively, given the boundary condition that the distributions should vanish for $\mu^2 = k_0^2$. In principle, everything is therefore given. In practice, the vector-meson distributions are not known, and so one is obliged to pick some reasonable ansatz with parameters fitted to the data. This is the approach taken in our SaS parameterizations [5]. By comparison, conventional distributions are defined for resolved processes only:

$$f_a^{\gamma,\mathrm{res}}(x,\mu^2) = f_a^{\gamma,\mathrm{VMD}}(x,\mu^2) + f_a^{\gamma,\mathrm{anom}}(x,\mu^2;k_0^2) \; . \tag{6}$$

These resolved distributions are then less constrained, in particular with respect to the momentum sum [12] of resolved partons.

3 Cross Sections

3.1 The total cross section and its subdivision

Total hadronic cross sections show a characteristic fall-off at low energies and a slow rise at higher energies. This behaviour can be parameterized by the form

$$\sigma_{\mathrm{tot}}^{AB}(s) = X^{AB} s^\epsilon + Y^{AB} s^{-\eta} \tag{7}$$

for $A + B \to X$. The powers ϵ and η are universal, with fit values [13]

$$\epsilon \approx 0.0808 \; , \qquad \eta \approx 0.4525 \; , \tag{8}$$

while the coefficients X^{AB} and Y^{AB} are process-dependent. Equation (7) can be interpreted within Regge theory, where the first term corresponds to pomeron exchange and gives the asymptotic rise of the cross section. Ultimately, this increase violates the Froissart–Martin bound [14]; ϵ should therefore be thought of as slowly decreasing with energy (owing to multi-pomeron exchange effects), although data at current energies are well fitted by a constant ϵ. The second term, the reggeon one, is mainly of interest at low energies. For the purpose of our study we do not rely on the Regge interpretation of eq. (7), but can merely consider it as a convenient parameterization.

The VMD part of the γp cross section should have a similar behaviour. The direct part reflects the parton distributions of the proton; a small-x behaviour like $xf(x) \sim x^{-\epsilon}$ would give $\sigma_{\rm dir}^{\gamma {\rm p}} \sim s^{\epsilon}$. The anomalous part is less easily classified: a purely perturbative description would not give a behaviour like VMD, but a duality argument with anomalous states interpreted in terms of higher vector-meson states would. Empirically, the γp data are well described by

$$\sigma_{\rm tot}^{\gamma {\rm p}}(s) \approx 67.7\, s^{\epsilon} + 129\, s^{-\eta} \quad [\mu{\rm b}], \tag{9}$$

with s in GeV^2. (Cross-sections are throughout given in mb for hadron–hadron interactions, in μb for γ–hadron ones and in nb for $\gamma\gamma$ ones.) Actually, the above formula is a prediction [13] preceding the HERA data [15, 16]. The conclusion would seem to be that, at least as far as total cross sections are concerned, the extended VMD description of anomalous interactions is a reasonable first approximation.

If we then take the Regge-theory ansatz seriously also for the photon, it is possible to derive an expression for the total $\gamma\gamma$ cross section

$$\sigma_{\rm tot}^{\gamma\gamma}(s) \approx 211\, s^{\epsilon} + 215\, s^{-\eta} \quad [{\rm nb}]. \tag{10}$$

This is based on the assumption that the pomeron and reggeon terms factorize, $X^{AB} = \beta_{A\mathbb{P}}\beta_{B\mathbb{P}}$ and $Y^{AB} = \gamma_{A\mathbb{R}}\gamma_{B\mathbb{R}}$, so that $X^{\gamma\gamma} = (X^{\gamma {\rm p}})^2/X^{\rm pp}$ and $Y^{\gamma\gamma} = 2(Y^{\gamma {\rm p}})^2/(Y^{\rm pp}+Y^{{\rm p}\overline{\rm p}})$, with $X^{\rm pp} \approx 21.70$ and $(Y^{\rm pp} + Y^{{\rm p}\overline{\rm p}})/2 \approx 77.23$. In hadronic cross sections, factorization seems valid for the pomeron term but not for the reggeon one, e.g. $X^{{\rm p}\overline{\rm p}} = X^{\rm pp}$ while $Y^{{\rm p}\overline{\rm p}} \approx 98.39 \gg Y^{\rm pp} \approx 56.08$. The choice of using the average of $Y^{\rm pp}$ and $Y^{{\rm p}\overline{\rm p}}$ then is an arbitrary one, though it can be motivated roughly by arguments of counting the number of allowed valence quark/antiquark annihilation/exchange diagrams possible in the various processes. The band of uncertainty can be obtained by using either $Y^{\rm pp}$ or $Y^{{\rm p}\overline{\rm p}}$ alone, i.e. $Y^{\gamma\gamma} = 297$ and 169. This ambiguity only affects the low-energy behaviour, and so is not critical for us. It is illustrated in Fig. 4, where we also compare with existing data on $\sigma_{\rm tot}^{\gamma\gamma}(s)$.

Note that factorization is assumed to hold separately for the pomeron and the reggeon terms, not for the total cross section itself. That is, the relation $\sigma_{\rm tot}^{\gamma\gamma} = 2(\sigma_{\rm tot}^{\gamma {\rm p}})^2/(\sigma_{\rm tot}^{\rm pp} + \sigma_{\rm tot}^{{\rm p}\overline{\rm p}})$ is not exact in this approach, although numerically it is a very good approximation (usually to better than 1%).

Our eq. (10) above should be compared with the time-honoured expression $\sigma^{\gamma\gamma} = 240 + 270/W$ [17]. This corresponds to a critical pomeron, $\epsilon = 0$, as was commonly assumed in the early seventies, and an $\eta = 0.5$, but it is otherwise in the same spirit as our formula. Also numerically the two closely agree at not too large energies, see Fig. 4.

One should remember that our expression (10) is here 'derived' based on a simple Regge-theory ansatz that has no real validity for the photon. Next we will proceed to study the contributions of the individual event classes. The constraints that come from γp physics data then directly feed into constraints on the contribution from these classes and therefore on the total $\gamma\gamma$ cross section. At the end of the day we will therefore show that a cross section behaving roughly like eq. (10) should be a good approximation. In doing so, the properties of the event classes are also fixed, to a large extent.

Based on the subdivision into event classes, the total γp cross section may be written as

$$\sigma_{\rm tot}^{\gamma {\rm p}} = \sigma_{\rm VMD}^{\gamma {\rm p}} + \sigma_{\rm dir}^{\gamma {\rm p}} + \sigma_{\rm anom}^{\gamma {\rm p}} \tag{11}$$

and the total $\gamma\gamma$ one as

$$\sigma_{\rm tot}^{\gamma\gamma} = \sigma_{\rm VMD\times VMD}^{\gamma\gamma} + 2\sigma_{\rm VMD\times dir}^{\gamma\gamma} + 2\sigma_{\rm VMD\times anom}^{\gamma\gamma} + \sigma_{\rm dir\times dir}^{\gamma\gamma} + 2\sigma_{\rm dir\times anom}^{\gamma\gamma} + \sigma_{\rm anom\times anom}^{\gamma\gamma} \ . \tag{12}$$

Here we explicitly keep the factor of 2 for the off-diagonal terms, where the rôle of the two incoming photons may be interchanged.

3.2 The VMD contributions

The Vp cross sections may be parameterized as

$$\sigma_{\rm tot}^{\rho^0{\rm p}} \approx \sigma_{\rm tot}^{\omega{\rm p}} \approx \frac{1}{2}\left(\sigma_{\rm tot}^{\pi^+{\rm p}} + \sigma_{\rm tot}^{\pi^-{\rm p}}\right) \approx 13.63\, s^{\epsilon} + 31.79\, s^{-\eta} \quad [{\rm mb}], \tag{13}$$

$$\sigma_{\rm tot}^{\phi{\rm p}} \approx \sigma_{\rm tot}^{{\rm K}^+{\rm p}} + \sigma_{\rm tot}^{{\rm K}^-{\rm p}} - \sigma_{\rm tot}^{\pi^-{\rm p}} \approx 10.01\, s^{\epsilon} - 1.51\, s^{-\eta} \quad [{\rm mb}]. \tag{14}$$

The ϕp cross section is not expected to have a reggeon term and indeed the additive quark model [19] formulae give a contribution close to zero; a small negative term could easily come from threshold effects and so we choose to keep it. Lacking measurements of Dp cross sections we cannot use the additive quark model to estimate the J/ψp cross section. The latter could in principle be extracted from data on J/ψ production in nuclear collisions. Superficially a value of about 6 mb at $5 \lesssim \sqrt{s} \lesssim 10$ GeV comes out but this value presumably is too large since in the so far accessible kinematical range of large positive x_F the J/ψ is formed outside the nucleus. Therefore we fix the VMD coupling of the J/ψ at its leptonic value and use a low-energy measurement of elastic J/ψ photoproduction to determine the J/ψp cross section. This implies a reduction of the ψp cross section by a factor of about 10 compared to the ϕp one, in agreement with the expectation that the soft pomeron couples more weakly to heavier quarks. Again using factorization for the pomeron and reggeon terms separately, the total cross section for two vector mesons is

$$\sigma_{\rm tot}^{V_1V_2} \approx \frac{X^{{\rm p}V_1} X^{{\rm p}V_2}}{X^{\rm pp}}\, s^{\epsilon} + \frac{2Y^{{\rm p}V_1} Y^{{\rm p}V_2}}{Y^{\rm pp} + Y^{{\rm p}\overline{\rm p}}}\, s^{-\eta} \ . \tag{15}$$

These X and Y coefficients are collected in Table 1.

The total VMD cross sections are obtained as weighted sums of the allowed vector-meson states,

$$\sigma_{\rm VMD}^{\gamma{\rm p}} = \sum_V \frac{4\pi\alpha_{\rm em}}{f_V^2}\, \sigma_{\rm tot}^{V{\rm p}} \approx 54\, s^{\epsilon} + 115\, s^{-\eta} \quad [\mu{\rm b}], \tag{16}$$

$$\sigma_{\rm VMD\times VMD}^{\gamma\gamma} = \sum_{V_1} \frac{4\pi\alpha_{\rm em}}{f_{V_1}^2} \sum_{V_2} \frac{4\pi\alpha_{\rm em}}{f_{V_2}^2}\, \sigma_{\rm tot}^{V_1V_2} \approx 133\, s^{\epsilon} + 170\, s^{-\eta} \quad [{\rm nb}]. \tag{17}$$

In Fig. 5 we show the breakdown of $\sigma_{\rm VMD\times VMD}^{\gamma\gamma}$ by vector-meson combination. Obviously the $\rho^0\rho^0$ combination dominates.

For a description of VMD events, a further subdivision into elastic (el), diffractive (sd and dd for single and double diffractive) and non-diffractive (nd) events is required. Keeping only the simplest diffractive topologies, one may write

$$\sigma_{\rm tot}^{AB}(s) = \sigma_{\rm el}^{AB}(s) + \sigma_{{\rm sd}(XB)}^{AB}(s) + \sigma_{{\rm sd}(AX)}^{AB}(s) + \sigma_{\rm dd}^{AB}(s) + \sigma_{\rm nd}^{AB}(s) \ . \tag{18}$$

The elastic and diffractive cross sections for all required Vp and V_1V_2 processes have been calculated and parameterized in the context of our model presented in ref. [20]. The same formulae are used as those collected in section 4 of that paper, and so are not

repeated here; only the expressions in its eq. (26) have to be replaced. The following parameterizations have been chosen:

$$
\begin{aligned}
M^2_{\mathrm{max},XB} &= c_1 s + c_2 \ , \\
B_{XB} &= c_3 + \frac{c_4}{s} \ , \\
M^2_{\mathrm{max},AX} &= c_5 s + c_6 \ , \\
B_{AX} &= c_7 + \frac{c_8}{s} \ , \\
\Delta_0 &= d_1 + \frac{d_2}{\ln s} + \frac{d_3}{\ln^2 s} \ , \\
M^2_{\mathrm{max},XB} &= s \left(d_4 + \frac{d_5}{\ln s} + \frac{d_6}{\ln^2 s} \right) \ , \\
B_{XX} &= d_7 + \frac{d_8}{\sqrt{s}} + \frac{d_9}{s} \ .
\end{aligned} \tag{19}
$$

The coefficients c_i and d_i are given in Table 1. Additionally the b slope parameters are $b_{\mathrm{p}} = 2.3$ GeV^{-2}, $b_\rho = b_\omega = b_\phi = 1.4$ GeV^{-2} and $b_{\mathrm{J}/\psi} = 0.23$ GeV^{-2}. The non-diffractive cross-section is then given by whatever is left. This subdivision is shown in Fig. 6 for the sum of all meson combinations, which then mainly reflects the $\rho^0\rho^0$ composition.

The σ_{nd} may be further subdivided into a low-$p_\perp$ and a high-$p_\perp$ class. Since the $2 \to 2$ parton–parton scattering cross sections are divergent in the limit $p_\perp \to 0$, some further care is needed for this classification. We expect the perturbative formulae to break down at small $p_\perp$, since an exchanged gluon with a large transverse wavelength $\lambda_\perp \sim 1/p_\perp$ cannot resolve the individual colour charges inside a hadron. The hadron being a net colour singlet, the effective coupling should therefore vanish in this limit. A parameter $p_{\perp\mathrm{min}} = p_{\perp\mathrm{min}}(s)$ is introduced to describe the border down to which the perturbative expression is assumed to be valid [4]. The jet rate above $p_{\perp\mathrm{min}}$ may still be large, in fact even larger than the total σ_{nd}. It is therefore necessary to allow for the possibility of having several perturbative parton–parton interactions in one and the same event, i.e. to unitarize the jet emission probability. We do this using the formalism of ref. [21]. A fit to collider multiplicities gives

$$
p_{\perp\mathrm{min}}(s) = p^{\mathrm{VMD}}_{\perp\mathrm{min}}(s) \approx 1.30 + 0.15 \, \frac{\ln(E_{\mathrm{cm}}/200)}{\ln(900/200)} \ \ [\mathrm{GeV}] \ . \tag{20}
$$

Here we uses the CTEQ 2L [22] leading-order parton distributions (extended to small x and Q^2 as described in [4]), with $p_\perp^2$ as scale choice.

3.3 The direct and anomalous contributions

Comparing eqs. (9) and (16), about 80% of the γp total cross section is seen to come from the VMD term. The remaining 20% is to be attributed to the direct and anomalous components. When applying a perturbative description, the anomalous part is negligible at small energies. The dependence of the direct cross section on k_0 can then be used to determine this parameter. We obtain a value of $k_0 \approx 0.5$ GeV [4], which is consistent with the simple-minded answer $k_0 \approx m_\phi/2$. In our study of the parton distributions of the photons [5] a reasonable $f_a^{\gamma,\mathrm{res}}(x,\mu^2)$ was obtained with $Q_0 = 0.6$ GeV, i.e. the same order. For this study we have stayed with the latter number, $k_0 = 0.6$ GeV.

The anomalous process contains two cut-off parameters, the k_0 scale for the photon to branch to a perturbative $q\overline{q}$ pair and a $p_{\perp\min}^{\rm anom}$ scale for one of the anomalous-photon partons to interact in a hard process. As a first guess, one might choose $p_{\perp\min}^{\rm anom}$ also to be given by eq. (20). However, this turns out to give a cross section increasing too rapidly at large energies. Physically, it is understandable why hard processes should be more suppressed at small $p_\perp$ in anomalous processes than in VMD ones: the anomalous photon corresponds to a $q\overline{q}$ pair of larger virtuality than a VMD one, and hence of smaller spatial extent, i.e. with larger potential for colour screening. The best recipe for including this physics aspect is not well understood. As a purely pragmatical recipe, one can pick $p_{\perp\min}^{\rm anom}(s)$ with an s dependence such that the VMD, direct and anomalous processes add up to the expected behaviour (9). Over the energy range $20 \lesssim \sqrt{s} \lesssim 1000$ a suitable parameterization then is

$$p_{\perp\min}^{\rm anom}(s) \approx 0.6 + 0.125\ \ln^2(1+\sqrt{s}/10)\ \ [\mathrm{GeV}]\ . \tag{21}$$

This is based on parton distributions SaS 1D [5] for the photon and CTEQ 2L for the proton, combined with lowest-order matrix elements. At low energies the results are fairly unstable to variations in k_0, and so the behaviour of $p_{\perp\min}^{\rm anom}(s)$ in this region should not be over-interpreted. The split of the γp cross section into VMD, direct and anomalous is shown in Fig. 7.

In this purely perturbative picture we have neither included any class of 'soft' anomalous interactions nor the possibility of multiple parton–parton interactions. Keeping everything else the same, the former would increase the cross section and the latter decrease it. However, when introducing a soft component, it is important to avoid double-counting. To illustrate the issue, consider the simple graph of Fig. 8a. There are two transverse momentum scales, $k_\perp$ and $p_\perp$. It is a simpler version of Fig. 3, with inessential gluons removed and for γp rather than $\gamma\gamma$, so has one scale less. The allowed phase space can then conveniently be represented by a two-dimensional plane, Fig. 8b. The region $k_\perp < k_0$ corresponds to a small transverse momentum at the $\gamma \to q\overline{q}$ vertex, and thus to VMD processes. For $k_\perp > k_0$, the events are split along the diagonal $k_\perp = p_\perp$. If $k_\perp > p_\perp$, the hard $2 \to 2$ process of Fig. 8a is $\gamma g \to q\overline{q}$, and the lower part of the graph is part of the leading log QCD evolution of the gluon distribution inside the proton. These events are direct ones. If $p_\perp > k_\perp$, on the other hand, the hard process is $\overline{q}q' \to \overline{q}q'$, and the $\gamma \to q\overline{q}$ vertex builds up the quark distribution inside a photon. These events are thus anomalous ones.

By analogy with the VMD representation, each fixed-$k_\perp$ component of $\gamma \leftrightarrow q\overline{q}$ fluctuations can be considered as a separate 'hadron species', with a density of states proportional to $\mathrm{d}k_\perp^2/k_\perp^2$. Each vertical 'tower' at some given $k_\perp$ scale would correspond to a higher excited vector resonance in the context of a generalized VMD model. In this tower, the soft events would be in the direct sector and the hard events in the anomalous sector. In the region of large $k_\perp$ values the perturbative language is well defined, and no problems should arise. As smaller and smaller $k_\perp$'s are considered, however, one could expect event properties that are intermediate to those of VMD. In particular, multiple parton–parton interactions could be possible, and this would affect the relation between calculated jet cross sections and the total event cross section. Previously we had to introduce a large $p_{\perp\min}^{\rm anom}$ scale at high energies to solve the problem of too large an anomalous cross section, which means we left an un-populated hole in the middle of Fig. 8b (indicated by a question mark). The hope is that multiple interactions would provide a natural resolution of this problem, in the sense that most anomalous events have one hard scattering above

$p_{\perp\min}^{\rm anom}$, while the anomalous region with $p_\perp < p_{\perp\min}^{\rm anom}$ does not significantly contribute new events but rather further interactions inside the events above.

The hope for a simple solution is not borne out by studies, however [7]. Eikonalization does dampen the increase of the anomalous and direct cross sections, but not enough. With a $p_{\perp\min}^{\rm anom}(s) = p_{\perp\min}^{\rm VMD}(s)$ the cross section is still increasing too fast at high energies, if the pomeron-style behaviour is taken as reference. Problems that appear already in the γp sector are even more severe in attempts at a $\gamma\gamma$ description along the same lines. It therefore seems clear that further aspects have to be taken into account, such as momentum conservation, coherence effects or strict geometrical cuts.

We intend to return to these problems, but for the moment stay with a purely perturbative description of the direct and anomalous components. By pushing this approach to its logical conclusion, we see what to expect from it and what limitations it has. Furthermore, for most event properties we expect the perturbative description to be perfectly adequate.

3.4 The total $\gamma\gamma$ cross section by component

Turning to the $\gamma\gamma$ cross sections, in principle all free parameters have now been fixed, and the cross section for each of the six event classes can be obtained. The VMD$\times$VMD one has already been discussed; the others are given as integrals of $2 \to 2$ scattering cross sections above the respective $p_\perp$ cut-offs already specified. The results are shown in Fig. 9, class by class. For comparison, we also show the results that would be obtained in a simple factorization ansatz

$$\sigma_{i\times j}^{\gamma\gamma} = \frac{2}{1+\delta_{ij}} \frac{2\,\sigma_i^{\gamma\rm p}\,\sigma_j^{\gamma\rm p}}{\sigma_{\rm tot}^{\rm pp} + \sigma_{\rm tot}^{\rm p\overline{p}}} \;, \tag{22}$$

where $i, j =$ VMD, direct and anomalous.

A few comments about each of the classes:

1. For the VMD$\times$VMD class in principle the simple factorization ansatz is exact in our model; some minor deviations come from the reggeon term.
2. The VMD$\times$direct class comes out about a factor 3/2 larger than expected from the factorized ansatz. This difference can be understood by comparing the jet and the total cross sections of a proton and a π meson, where the latter is taken as a prototype for a VMD meson. Both the p and the π have parton distributions normalized to unit momentum sum, and the same small-x behaviour (using our prescription [4]). Neglecting some differences in the shape of the parton distributions, the jet rates therefore are comparable between pp, πp and $\pi\pi$ collisions. The total cross sections, on the other hand, are scaled down roughly by a factor 2/3 between pp and πp. Therefore the jet rate per event is a factor 3/2 larger for πp than for pp, and it is this factor that appears above. That is, eq. (22) would have worked only if $\gamma\pi/\pi\pi$ cross sections could have been used rather than γp/pp ones. The larger jet rate per event for mesons should be reflected in differences in the eikonalization treatment of the direct and anomalous components of γp and $\gamma\pi$ events.
3. The VMD$\times$anomalous component gives exactly the same factor 3/2 mismatch as discussed above for the VMD$\times$direct one.
4. The direct$\times$direct component is not at all well predicted by the factorized ansatz. The latter yields a cross section growing at large energies at a rate related to the

small-x behaviour of the proton distribution functions, i.e. $\propto s^{\epsilon}$ for our modified distributions. On the other hand, the total cross section for $\gamma\gamma \to \mathrm{q\overline{q}}$ is proportional to $\ln(s/k_0^2)/s$, and thus drops rapidly with c.m. energy.

5. The direct×anomalous component compares reasonably well with the prediction from factorization.
6. The anomalous×anomalous process, finally, is most uncertain, since it completely involves the interactions of the least well understood component of the photon wave function.

In Fig. 10 the total $\gamma\gamma$ cross section is compared between the Regge type ansatz (10) and the sum of the six classes above, eq. (12). It should be remembered that the first three are the dominant ones. In fact, since the direct and anomalous components together give about 20% of the γp total cross section, the expectation is that the last three classes together would only give a 4% contribution to the total $\gamma\gamma$ cross section. The anomalous×anomalous component may give a somewhat larger contribution than expected, but still the 4% number gives the right ballpark. The first three classes, on the other hand, are all related to the respective γp classes, with only a replacement of a p by a V (and an extra weight factor $4\pi\alpha_{\mathrm{em}}/f_V^2$). Apart from the appearance of a factor 3/2 in the VMD×direct and VMD×anomalous components, which should (largely if not completely) go away in a fully eikonalized description, these components behave as expected. This makes the argumentation for eq. (10) credible. However, if one wants to take a conservative approach, the spread between the two curves in Fig. 10 could be viewed as a band of uncertainty. The data are not yet precise to provide any discrimination, cf. Fig. 4.

One can also compare our $\sigma_{\mathrm{tot}}^{\gamma\gamma}$ with the numbers obtained in various minijet-based approaches [9, 3]. For $E_{\mathrm{cm}} = 200$ GeV, cross sections in the range 1000–1800 nb are typically obtained, but are reduced to about 500 nb if unitarity is enforced, in agreement with our results.

4 Event Properties

The subdivision of the total γp and $\gamma\gamma$ cross sections above, with the related choices of cut-off parameters etc., specifies the event composition at the hard-scattering level. Some interesting observables can be based on this classification alone. For instance, Fig 11 gives the cross section for elastic events of the kinds $\rho^0\rho^0$, $\rho^0\omega$, $\rho^0\phi$ and $\rho^0\mathrm{J}/\psi$. The former three processes are good tests for the validity of the VMD ansatz, whereas the last one could provide new insights.

For most studies it is necessary to consider the complete event structure, i.e. to add models for initial- and final-state QCD radiation (parton showers), for beam remnants, and for fragmentation and secondary decays [4]. A Monte Carlo generation of complete hadronic final states is obtained with PYTHIA/JETSET [23]. Thus any experimental quantity can be studied. This section gives some representative examples. In particular, we compare the properties of pp, γp and $\gamma\gamma$ events. It should be noted that pp and $\mathrm{p\overline{p}}$ events are very similar for the quantities studied here. Unless otherwise specified, the figures refer to an $E_{\mathrm{cm}} = \sqrt{s_{\gamma\gamma}} = 200$ GeV. As we will show at the end of the section, the qualitative features do not depend critically on this choice. Furthermore, figures relevant for LEP 2 energies can be found in the proceedings of the LEP 2 workshop [3, 24], so it makes sense to complement here with the higher-energy behaviour relevant for future

linear colliders.

Figure 12 shows the total transverse energy per event for each of the six components of the $\gamma\gamma$ cross section. The spike at small $\sum E_\perp$ for the VMD$\times$VMD class comes from elastic scattering events, e.g. $\gamma\gamma \to \rho^0\rho^0$. Also diffractive events contribute in this region. The large-$\sum E_\perp$ tail of the VMD$\times$VMD curve is enhanced by the possibility of multiple parton–parton interactions, which is only included for this class currently. Because of the larger $p_{\perp\min}^{\mathrm{anom}}$ cut-off, the classes involving anomalous photons typically have larger $\sum E_\perp$, while the smaller p_0 cut-off for the direct processes corresponds to smaller median $\sum E_\perp$. However, note that the $\gamma\gamma \to \mathrm{q\overline{q}}$ processes only fall off very slowly with $p_\perp$, in part because of the absence of structure functions, in part because of the form of the matrix element itself. The direct$\times$direct class therefore wins out at very large $\sum E_\perp$.

The results of Fig. 12 are a bit misleading, since the relative importance of the six event classes is not visible. The weighted mixture is shown in Fig. 13, also compared with γp and pp events. One observes a steady progression, with $\langle \sum E_\perp \rangle_{\mathrm{pp}} < \langle \sum E_\perp \rangle_{\gamma\mathrm{p}} < \langle \sum E_\perp \rangle_{\gamma\gamma}$. This pattern, of more activity for a γ than for a p, is seen in essentially all distributions. The elastic spike at small $\sum E_\perp$ is less pronounced for $\gamma\gamma$, owing to three factors: the VMD$\times$VMD component is only a part of the $\gamma\gamma$ cross section, elastic scattering is a smaller fraction of the total $\rho^0\rho^0$ cross section than it is for pp, and kinetic energy in the $\rho^0 \to \pi^+\pi^-$ decays add to the total transverse energy.

The $E_\perp$ flow as a function of pseudorapidity, $\mathrm{d}E_\perp/\mathrm{d}\eta$, is given in Fig. 14. It illustrates how γp interpolates between pp and $\gamma\gamma$: around the direction of the incoming photon, the γp events look like the $\gamma\gamma$ ones, while they look more like pp ones in the opposite direction, with an intermediate behaviour in the central region. Since elastic and single diffractive events are likely to be removed from 'minimum-bias' data samples, Fig. 15 shows the behaviour without those two event classes. The quantitative $\gamma\gamma/\gamma\mathrm{p}/\mathrm{pp}$ differences then are slightly reduced, but qualitatively remain unchanged. Also in subsequent figures these events have been removed, and the same comment can be made there.

The charged-multiplicity distributions follow essentially the same pattern as shown for the $\sum E_\perp$ ones in Figs. 12–15, and are therefore not included here. There is one noteworthy exception, however: the direct$\times$direct component does not have a tail out to large multiplicities. That is, even if the process $\gamma\gamma \to \mathrm{q\overline{q}}$ can generate large $p_\perp$ values, the absence of any beam jets keeps the multiplicity down.

The transverse momentum spectrum of charged particles is shown in Fig. 16. The larger high-$p_\perp$ tail of the $\gamma\gamma$ processes is one of the simplest observables to experimentally establish differences between pp, γp and $\gamma\gamma$. Of course, the cause of the differences is to be sought in the higher jet rates associated with photon interactions. The jet spectra are compared in Fig. 17, using a simple cone algorithm where a minimum $E_\perp$ of 5 GeV is required inside a cone of $\Delta R = \sqrt{(\Delta\eta)^2 + (\Delta\phi)^2} < 1$. Already for an $E_{\perp\mathrm{jet}}$ of 5 GeV there are more than three times as many jets in $\gamma\gamma$ as in pp, and this ratio then increases with increasing $E_{\perp\mathrm{jet}}$. The spectacular differences in the jet rate at large $p_\perp$ are highlighted in Fig. 18. They mainly come about because the direct component involves the full energy of the incoming photon. The pseudorapidity distribution of jets is shown in Fig. 19. As in the inclusive $\mathrm{d}E_\perp/\mathrm{d}\eta$ distributions, the difference in behaviour between the γ and p hemispheres is readily visible.

To illustrate the energy dependence of these distributions, Fig. 20 gives the $\mathrm{d}E_\perp/\mathrm{d}\eta$ flow for c.m. energies of 50 GeV. This can be compared with the result for 200 GeV in Fig. 15. Qualitatively, the same pattern is seen at both energies, although relative differences tend to be somewhat reduced at larger energies. This is also true for other

observables, such as jet rates. One reason is that the possibility of multiple parton–parton interactions in the VMD component pushes up the activity in those events at larger energies, and thus brings them closer to the anomalous class. The importance of the direct class, on the other hand, is reduced at large energies. Further, at large energies, jet production is dominantly initiated by small-x incoming partons, where the VMD and anomalous distributions are more similar than at large x (although still different).

5 Summary and Outlook

In this paper we have shown that our model for γp events [4] can be consistently generalized to $\gamma\gamma$ events. That is, essentially all free parameters are fixed by (low-energy) γp phenomenology. Since we start out with a more detailed subdivision of the γp total cross section than has conventionally been done in the past, our $\gamma\gamma$ model also contains a richer spectrum of possible processes. We distinguish six main event classes, but most of these contain further subdivisions. The aim is that this approach will allow predictions for a broader range of observables than is addressed in conventional models. For instance, although not discussed in detail here, our approach does correlate the hard-jet physics in the central rapidity region with the structure of the beam remnants.

This does not mean that all results are complicated. We have shown that the simple Regge-theory expression $\sigma_{\mathrm{tot}}^{\gamma\gamma}(s) \approx 211\, s^{0.08} + 215\, s^{-0.45}$ [nb] comes close to what is obtained in our full analysis, and have a fair understanding where differences come from. We therefore expect this expression to be good to better than 10% from a few GeV onwards, at least to the top $\gamma\gamma$ energies that could be addressed with the next generation of linear $\mathrm{e^+e^-}$ colliders. Also global event properties show a very simple pattern, with more activity (transverse energy, multiplicity, jets, ...) in γp events than in pp ones, and still more in $\gamma\gamma$ ones. This is perhaps contrary to the naïve image of a 'clean' point-like photon. The γp events show their intermediate status by having a photon (proton) hemisphere that looks much like $\gamma\gamma$ (pp) events, with a smooth interpolation in the middle.

In our current model the perturbative approach to the description of the direct and anomalous components is pushed to its extreme. In this sense it is a useful study. However, we also see that it has its limitations: at high energies a purely perturbative treatment of the direct and anomalous components is no longer possible and unitarity corrections have to be taken into account, possibly through an eikonalized treatment of the two components along the lines indicated above (i.e. treating the direct event class as the soft component of the anomalous one). The goal is a consistent treatment covering the whole $(k_{\perp 1}, k_{\perp 2}, p_\perp)$ volume of $\gamma\gamma$ events in a consistent fashion, with smooth transitions between the various regions. Unfortunately this is a not so trivial task, and anyway must be based on input from the simpler model above. The current model therefore is a useful step towards an improved understanding of the photon and its interactions.

Also many other aspects need to be studied. Disagreements between the HERA data and our model can be found for the profile of beam jets, the structure of underlying events, the event topology composition and so on, indicating the need for further refinements [2]. The transition from a real γ to a virtual γ^* is still not well understood. Production in diffractive systems currently attract much attention. Further issues could be mentioned, but the conclusion must be that much work remains before we can claim to have a complete overview of the physics involved in γp and $\gamma\gamma$ events, let alone understand all the details.

References

[1] Proc. 8$^{\rm th}$ Int. Workshop on Photon–Photon Collisions, Shoresh, Israel, 1988, ed. U. Karshon (World Scientific, Singapore, 1988);
Proc. 9$^{\rm th}$ Int. Workshop on Photon–Photon Collisions, La Jolla, CA, USA, 1992, eds. D.O. Caldwell and H.P. Paar (World Scientific, Singapore, 1992);
Proc. Workshop on Two-Photon Physics from DAΦNE to LEP200 and Beyond, Paris, France, 1994, eds. F. Kapusta and J. Parisi (World Scientific, Singapore, 1994);
Proc. Workshop on Two-Photon Physics at LEP and HERA, Lund, Sweden, 1994, eds. G. Jarlskog and L. Jönsson (Fysiska Institutionen, Lunds Universitet, Lund, 1994);
Proc. Photon '95, Sheffield, U.K., 1995, eds. D.J. Miller, S.L. Cartwright and V. Khoze (World Scientific, Singapore, 1995)

[2] A. Levy, DESY–95–204, to appear in Proc. EPS HEP 95, Brussels, Belgium, 1995, and references therein;
Proc. Workshop on HERA Physics, Durham, U.K., 1995, in preparation

[3] Report on '$\gamma\gamma$ Physics', conveners P. Aurenche and G.A. Schuler, in Proc. Physics at LEP2, eds. G. Altarelli, T. Sjöstrand and F. Zwirner, CERN 96–01, Vol. 1, p. 291

[4] G.A. Schuler and T. Sjöstrand, Phys. Lett. **B300** (1993) 169, Nucl. Phys. **B407** (1993) 539

[5] G.A. Schuler and T. Sjöstrand, Z. Phys. **C68** (1995) 607; CERN–TH/96–04 and LU TP 96–2, to appear in Phys. Lett. **B**

[6] G.A. Schuler and T. Sjöstrand, in Proc. Workshop on Two-Photon Physics from DAΦNE to LEP200 and Beyond, Paris, France, 1994, eds. F. Kapusta and J. Parisi (World Scientific, Singapore, 1994), p. 163;
G.A. Schuler, in Proc. Workshop on Two-Photon Physics at LEP and HERA, Lund, Sweden, 1994, eds. G. Jarlskog and L. Jönsson (Fysiska Institutionen, Lunds Universitet, Lund, 1994), p. 200

[7] T. Sjöstrand, in Proc. XXIV International Symposium on Multiparticle Dynamics 1994, Vietri sul Mare, Italy, 1994, eds. A. Giovannini, S. Lupia and R. Ugoccioni (World Scientific, Singapore, 1995), p. 221;
T. Sjöstrand, in Proc. Photon '95, Sheffield, U.K., 1995, eds. D.J. Miller, S.L. Cartwright and V. Khoze (World Scientific, Singapore, 1995), p. 340

[8] C. Peterson, T.F. Walsh and P.M. Zerwas, Nucl. Phys. **B229** (1983) 301;
J.H. Field, F. Kapusta and L. Poggioli, Z. Phys. **C36** (1987) 121;
P. Aurenche et al., Nucl. Phys. **B286** (1987) 553

[9] M. Drees and R.M. Godbole, Nucl. Phys. **B339** (1990) 355, Z. Phys. **C59** (1993) 591;
J.R. Forshaw and J.K. Storrow, Phys. Rev. **D46** (1992) 4955

[10] P. Aurenche et al., Phys. Rev. **D45** (1992) 92;
A. Capella et al., Phys. Rep. **236** (1994) 227;
P. Aurenche et al., Comput. Phys. Commun. **83** (1994) 107;
R. Engel, Z. Phys. **C66** (1995) 203;

[11] T.H. Baur et al., Rev. Mod. Phys. **50** (1978) 261

[12] G.A. Schuler, CERN–TH/95–153 (1995)

[13] A. Donnachie and P.V. Landshoff, Phys. Lett. **B296** (1992) 227

[14] M. Froissart, Phys. Rev. **123** (1961) 1053;
A. Martin, Phys. Rev. **124** (1963) 1432

[15] ZEUS Collaboration, M. Derrick et al., Phys. Lett. **B293** (1992) 465;
H1 Collaboration, T. Ahmed et al., Phys. Lett. **B299** (1993) 374

[16] ZEUS Collaboration, M. Derrick et al., Z. Phys. **C63** (1994) 391;
H1 Collaboration, S. Aid et al., Z.Phys. **C69** (1995) 27

[17] J.L. Rosner, in 'ISABELLE Physics Prospects', BNL Report 17522 (1972), p. 316

[18] S.E. Baru et al., Z. Phys. **C53** (1992) 219, and references therein;
H.-J. Behrend et al., Z. Phys. **C51** (1991) 365

[19] E.M. Levin and L.L. Frankfurt, JETP Letters **2** (1965) 65;
H.J. Lipkin and F. Scheck, Phys. Rev. Lett. **16** (1966) 71;
H. Joos, Phys. Lett. **24B** (1967) 103;
J.J.J. Kokkedee, 'The Quark Model' (W.A. Benjamin, New York, 1969)

[20] G.A. Schuler and T. Sjöstrand, Phys. Rev. **D49** (1994) 2257

[21] T. Sjöstrand and M. van Zijl, Phys. Rev. **D36** (1987) 2019

[22] CTEQ Collaboration, H.L. Lai et al., Phys. Rev. **D51** (1995) 4763

[23] T. Sjöstrand, Comput. Phys. Commun. **82** (1994) 74

[24] Report on '$\gamma\gamma$ Event Generators', conveners L. Lönnblad and M. Seymour, in Proc. Physics at LEP2, eds. G. Altarelli, T. Sjöstrand and F. Zwirner, CERN 96–01, Vol. 2, p. 187

	ρ^0p	ϕp	J/ψp	$\rho^0\rho^0$	$\phi\rho^0$	J/$\psi\rho^0$	$\phi\phi$	J/$\psi\phi$	J/ψJ/ψ
X	13.63	10.01	0.970	8.56	6.29	0.609	4.62	0.447	0.0434
Y	31.79	−1.51	−0.146	13.08	−0.62	−0.060	0.030	−0.0028	0.00028
c_1	0.213	0.213	0.213	0.267	0.267	0.267	0.232	0.232	0.115
c_2	0	0	7	0	0	6	0	6	5.5
c_3	−0.47	−0.47	−0.55	−0.46	−0.48	−0.56	−0.48	−0.56	−0.58
c_4	150	150	800	75	100	420	110	470	570
c_5	0.267	0.232	0.115	0.267	0.232	0.115	0.232	0.115	0.115
c_6	0	0	0	0	0	0	0	0	5.5
c_7	−0.47	−0.47	−0.47	−0.46	−0.46	−0.50	−0.48	−0.52	−0.58
c_8	100	110	110	75	85	90	110	120	570
d_1	3.11	3.12	3.13	3.11	3.11	3.12	3.11	3.18	4.18
d_2	−7.10	−7.43	−8.18	−6.90	−7.13	−7.90	−7.39	−8.95	−29.2
d_3	10.6	9.21	−4.20	11.4	10.0	−1.49	8.22	−3.37	56.2
d_4	0.073	0.067	0.056	0.078	0.071	0.054	0.065	0.057	0.074
d_5	−0.41	−0.44	−0.71	−0.40	−0.41	−0.64	−0.44	−0.76	−1.36
d_6	1.17	1.41	3.12	1.05	1.23	2.72	1.45	3.32	6.67
d_7	−1.41	−1.35	−1.12	−1.40	−1.34	−1.13	−1.36	−1.12	−1.14
d_8	31.6	36.5	55.2	28.4	33.1	53.1	38.1	55.6	116.2
d_9	95	132	1298	78	105	995	148	1472	6532

Table 1: Coefficients of the total and partial Vp and V_1V_2 cross sections, according to the formulae given in the text, eqs. (7) and (19). The ω is not shown separately, since it is assumed to have the same behaviour as the ρ^0.

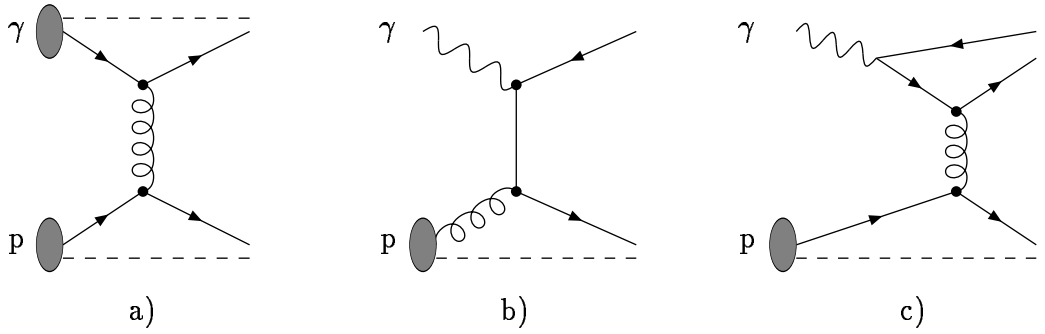

Figure 1: Contributions to hard γp interactions: a) VMD, b) direct, and c) anomalous. Only the basic graphs are illustrated; additional partonic activity is allowed in all three processes. The presence of spectator jets has been indicated by dashed lines, while full lines show partons that (may) give rise to high-$p_\perp$ jets.

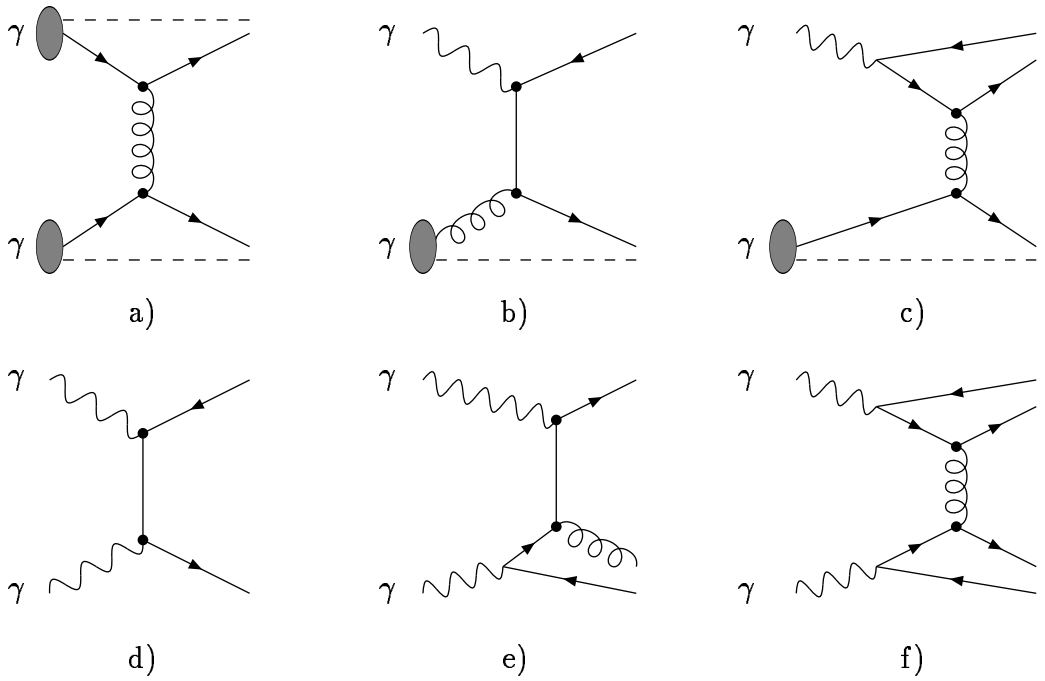

Figure 2: The six classes contributing to hard $\gamma\gamma$ interactions: a) VMD$\times$VMD, b) VMD$\times$direct, c) VMD$\times$anomalous, d) direct$\times$direct, e) direct$\times$anomalous, and f) anomalous$\times$anomalous. Notation as in Fig. 1.

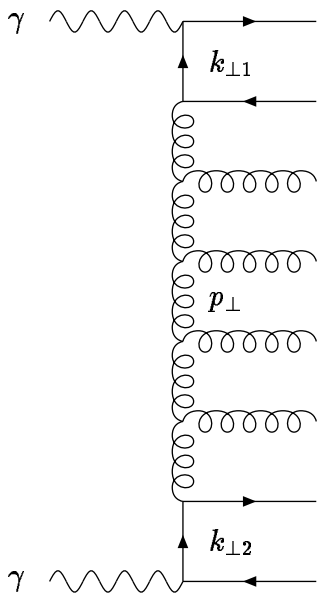

1. VMD×VMD: $k_{\perp 1}, k_{\perp 2} < k_0$, arbitrary $p_\perp$
2. VMD×dir: $k_{\perp 1} < k_0 \ll p_\perp \ll k_{\perp 2} + (1 \leftrightarrow 2)$
3. VMD×anom: $k_{\perp 1} < k_0 \ll k_{\perp 2} \ll p_\perp + (1 \leftrightarrow 2)$
4. dir×dir: $k_0 \ll k_{\perp 1} = k_{\perp 2}$
5. dir×anom: $k_0 \ll k_{\perp 1} \ll p_\perp \ll k_{\perp 2} + (1 \leftrightarrow 2)$
6. anom×anom: $k_0 \ll k_{\perp 1}, k_{\perp 2} \ll p_\perp$

Figure 3: A generic Feynman diagram (in the leading-log approximation) for $\gamma\gamma$ interactions and its decomposition into six components.

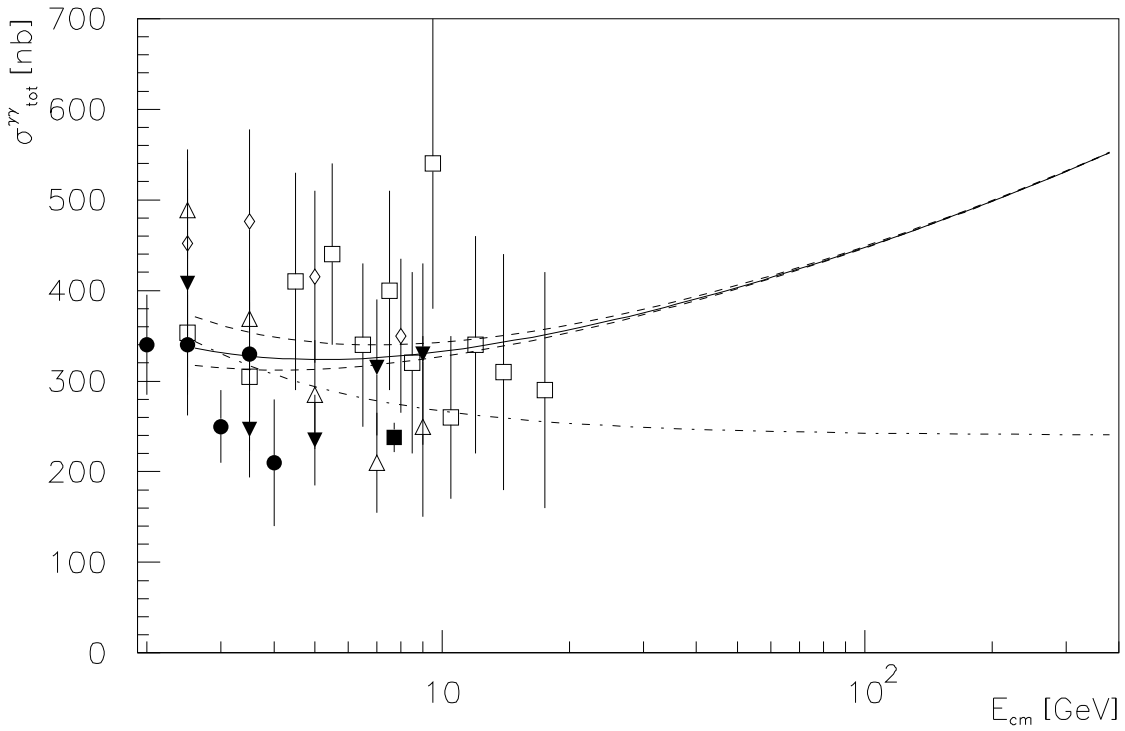

Figure 4: The total $\gamma\gamma$ cross section. Full curve: the parameterization of eq. (10). Dashed curves: range obtained by varying $Y^{\gamma\gamma}$ as described in the text. Dashed-dotted curve: the critical-pomeron parameterization [17]. Data points: open triangles PLUTO 1984, filled triangles PLUTO 1986, squares TPC/2γ 1985, spades TPC/2γ 1991, circles MD-1 1991, full square CELLO 1991 [18].

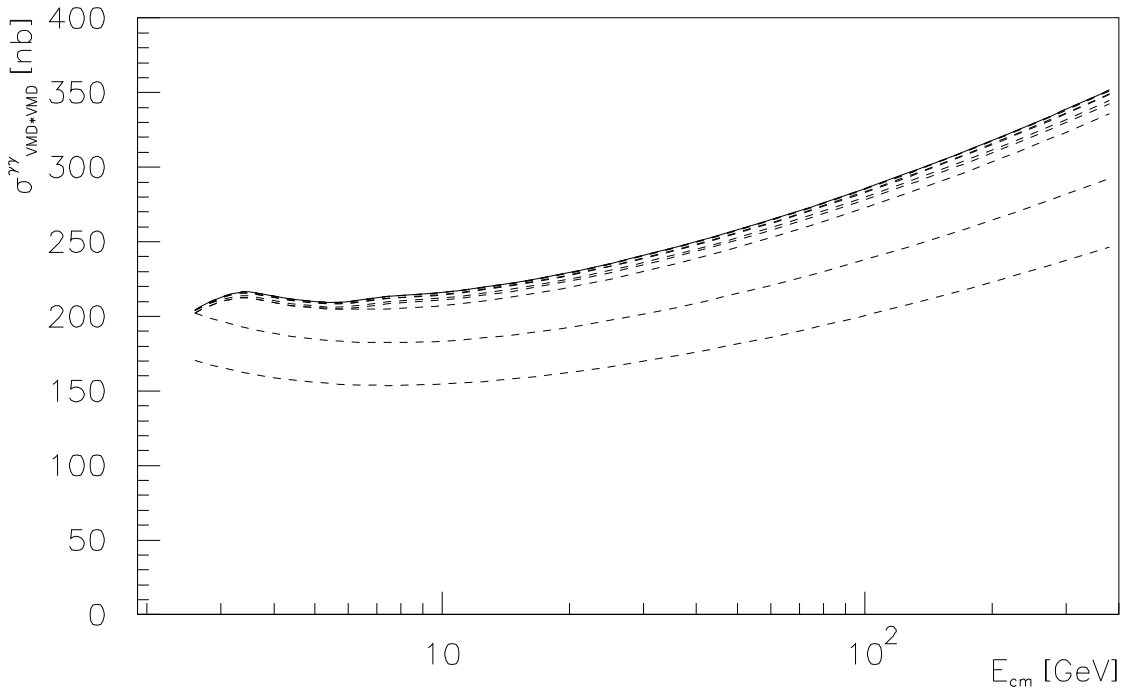

Figure 5: The total VMD$\times$VMD cross section, full curve, and its subdivision by vector-meson combination. The components are separated by dashed curves, from bottom to top: $\rho^0\rho^0$, $\rho^0\omega$, $\rho^0\phi$, $\rho^0\mathrm{J}/\psi$, $\omega\omega$, $\omega\phi$, $\omega\mathrm{J}/\psi$, $\phi\phi$, $\phi\mathrm{J}/\psi$, and $\mathrm{J}/\psi\mathrm{J}/\psi$. Some of the latter components are too small to be resolved in the figure.

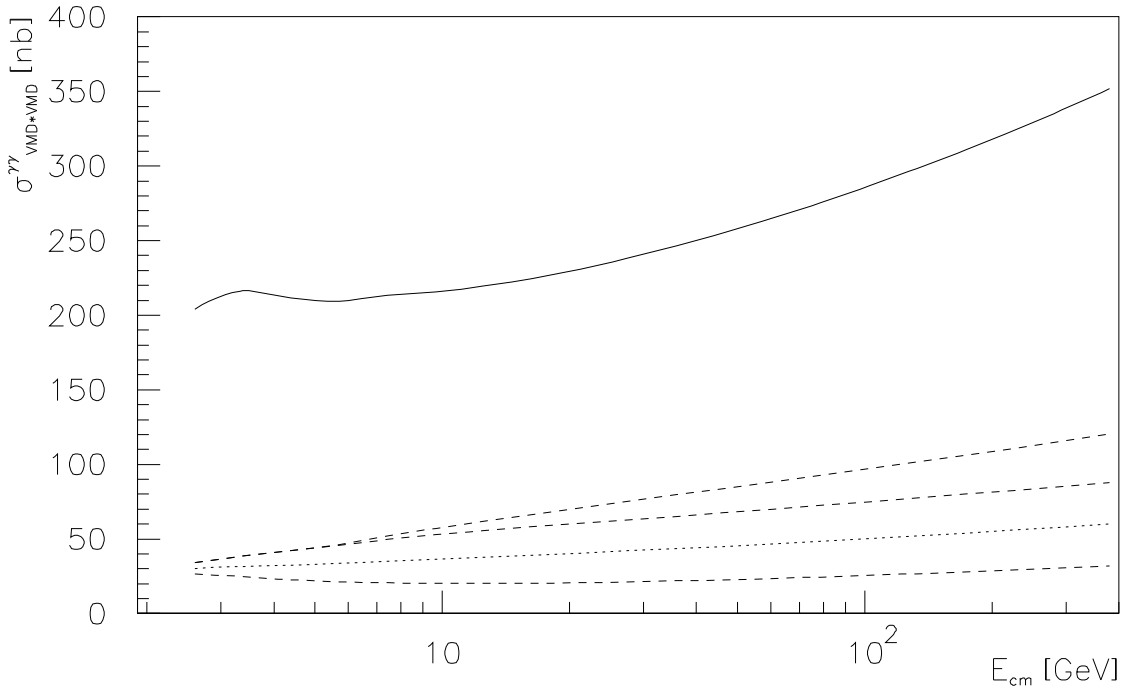

Figure 6: The total VMD$\times$VMD cross section, full curve, and its subdivision by event topology. The components are separated by dashed curves, from bottom to top: elastic, single diffractive (split for the two sides by the dotted curve), double diffractive, and non-diffractive (including jet events unitarized).

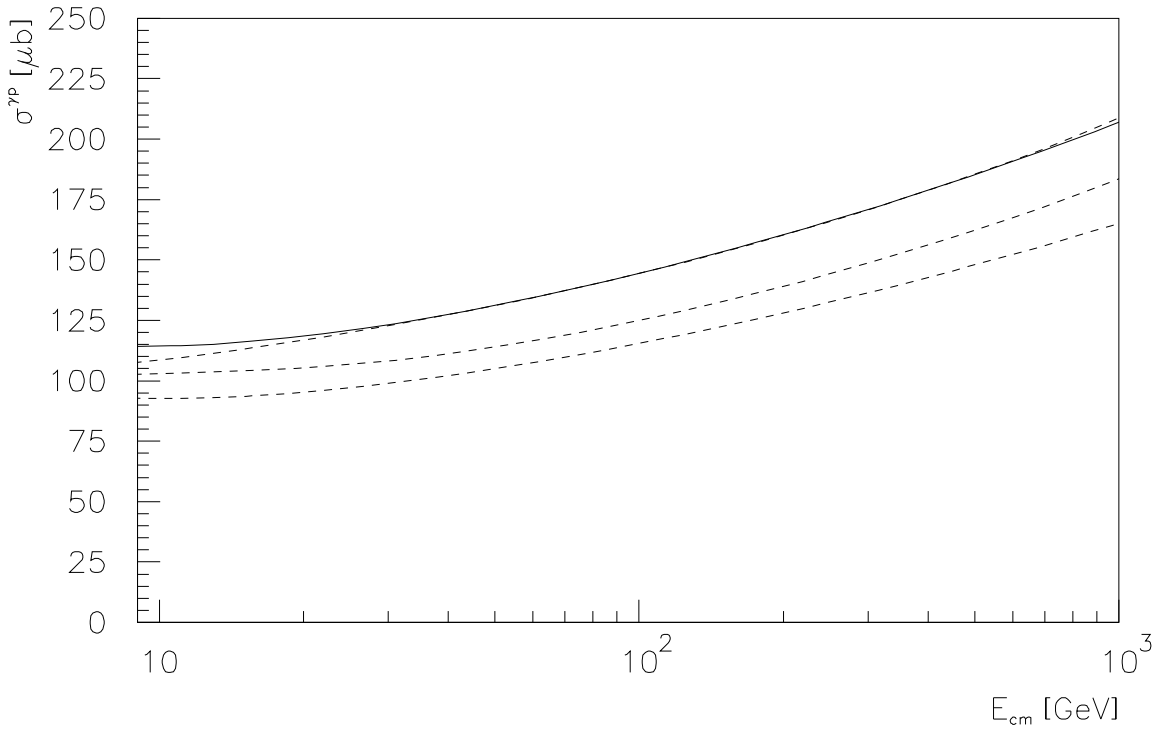

Figure 7: Components of the γp cross section: lower dashed curve the VMD contribution, middle dashed VMD+direct and upper dashed VMD+direct+anomalous, as obtained by integration with $k_0 = 0.6$ GeV and the $p_{\perp\min}^{\text{anom}}(s)$ of eq. (21). By comparison, full curve is the parameterization of eq. (9).

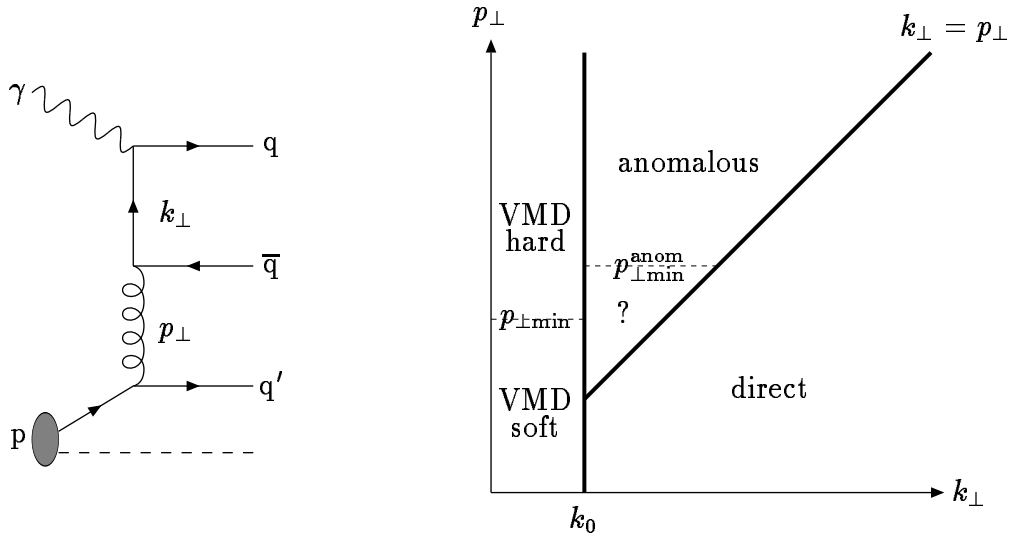

Figure 8: (a) Schematic graph for a hard γp process, illustrating the concept of two different scales. (b) The allowed phase space for this process, with the subdivision into event classes.

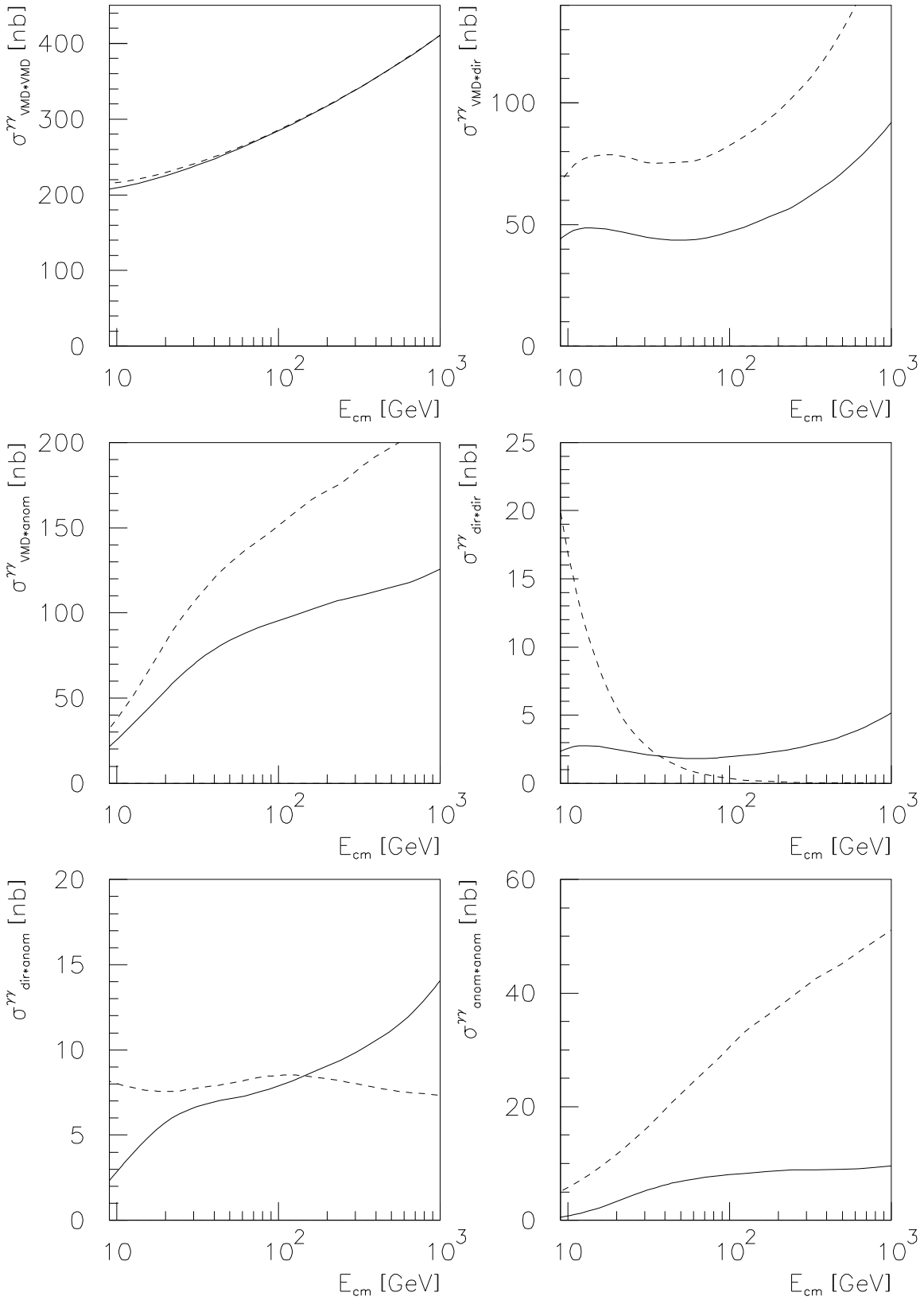

Figure 9: Comparison of $\gamma\gamma$ partial cross sections. Full curves: the simple factorization ansatz of eq. (22). Dashed curves: by integration of jet cross sections (except VMD$\times$VMD, where eq. (17) is used).

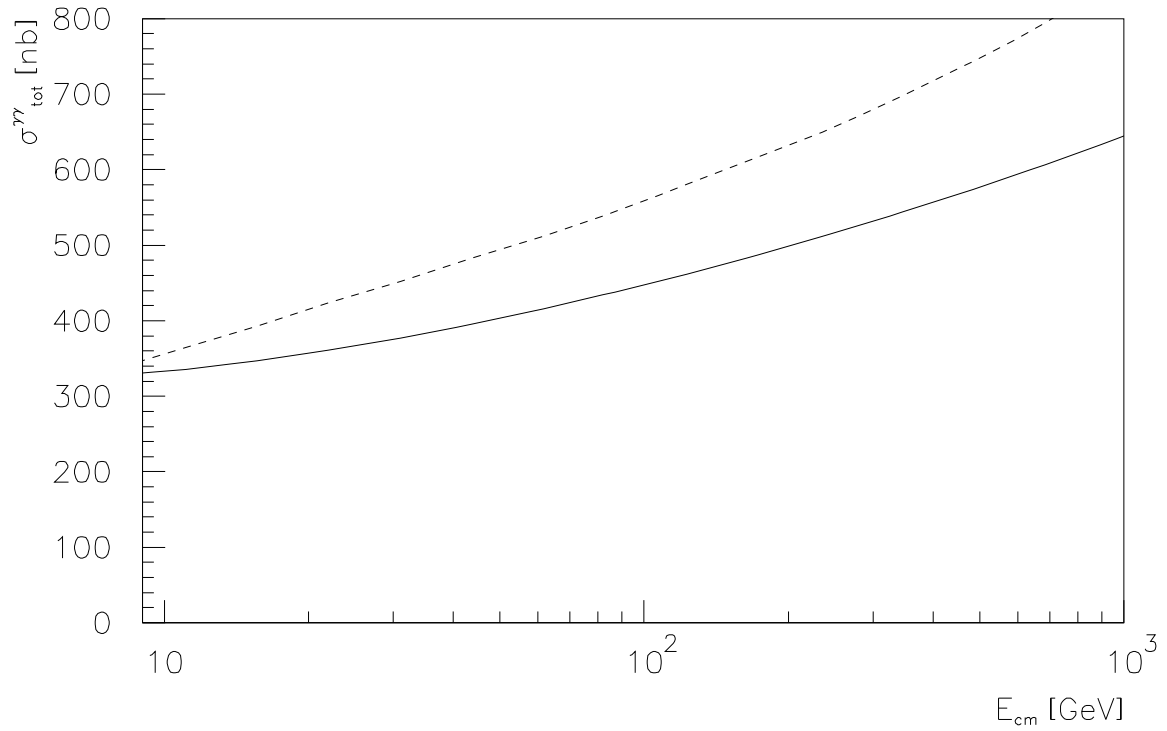

Figure 10: The total $\gamma\gamma$ cross section. Full curve: the parameterization of eq. (10). Dashed curve: result from sum of integrations of the six components.

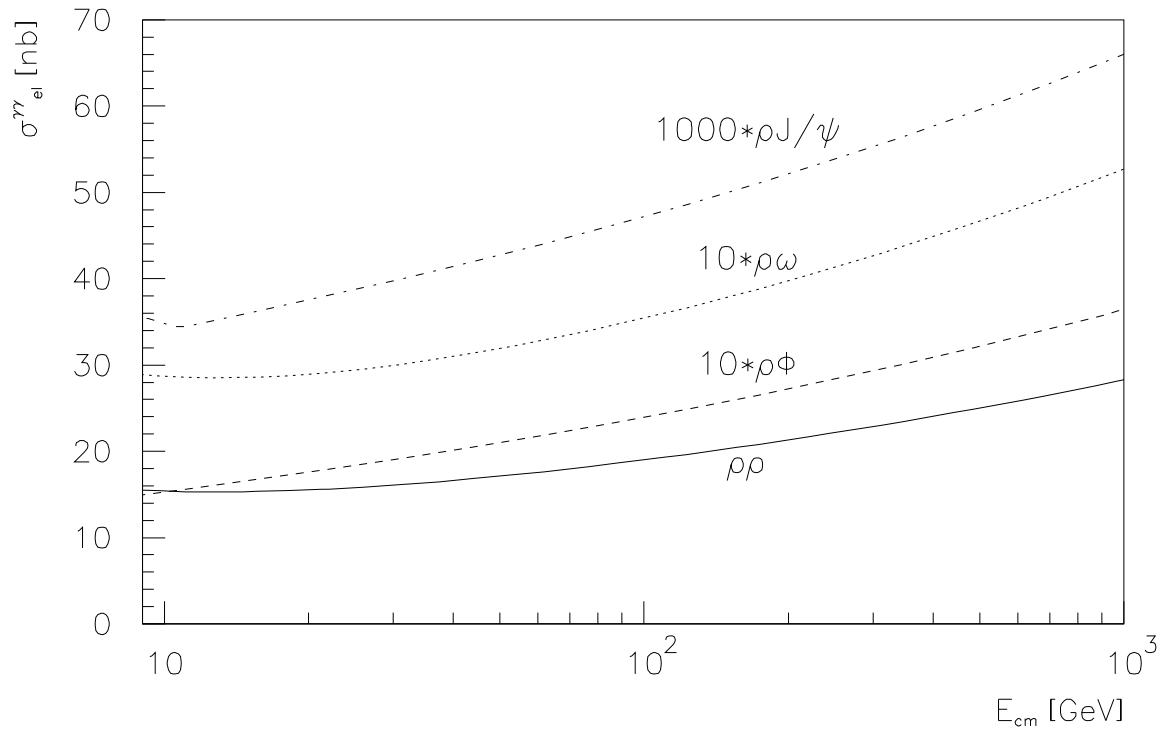

Figure 11: Elastic cross sections: $\rho^0\rho^0$ full curve, $\rho^0\omega$ dotted, $\rho^0\phi$ dashed and $\rho^0 J/\psi$ dash-dotted. The latter three cross sections include both mirror-symmetric configurations, and have additionally been scaled up by factors 10, 10 and 1000, respectively, for better visibility.

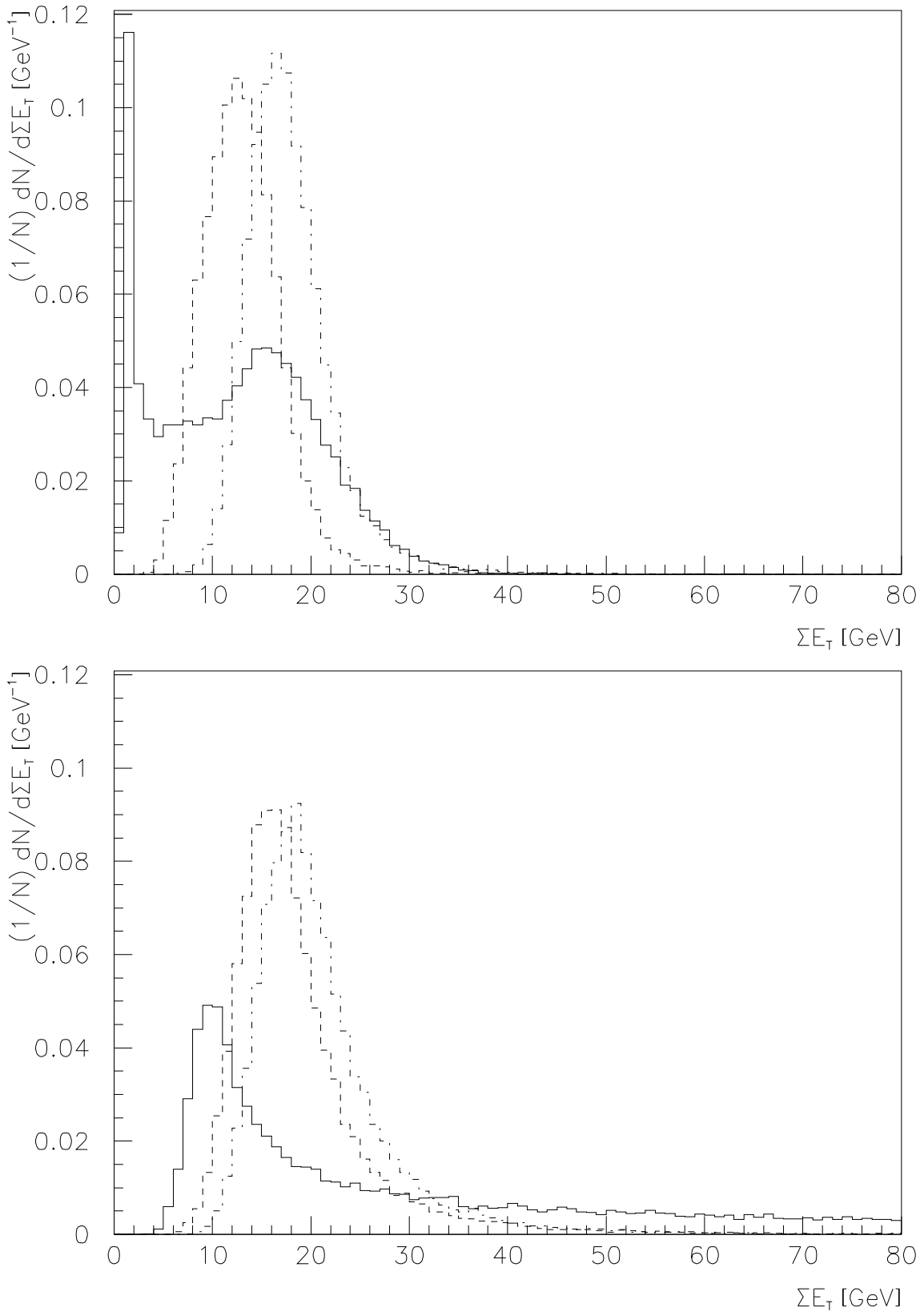

Figure 12: The total transverse energy per event, separately normalized for each of the six event classes. Top frame: VMD×VMD: full histogram; VMD×direct: dashed one; and VMD×anomalous: dash-dotted one. Bottom frame: direct×direct: full histogram; direct×anomalous: dashed one; and anomalous×anomalous: dash-dotted one.

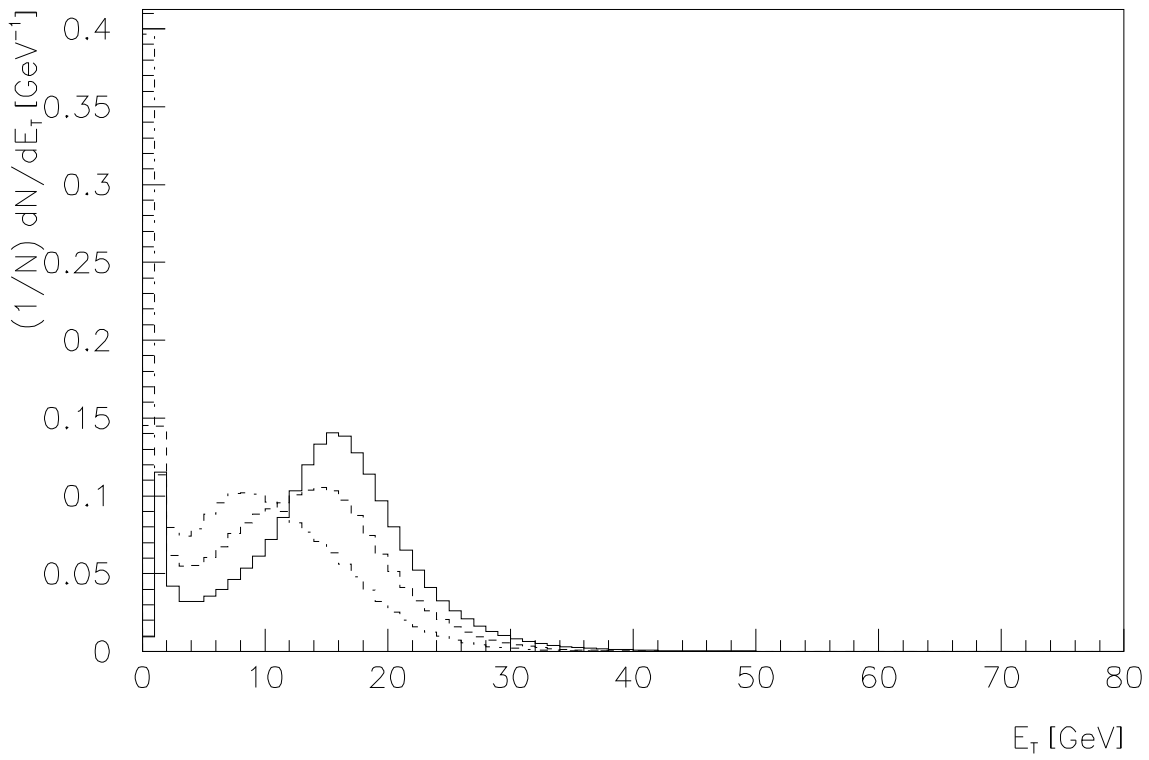

Figure 13: The total transverse energy per event for different beams: $\gamma\gamma$: full histogram; γp: dashed one: and pp: dash-dotted one.

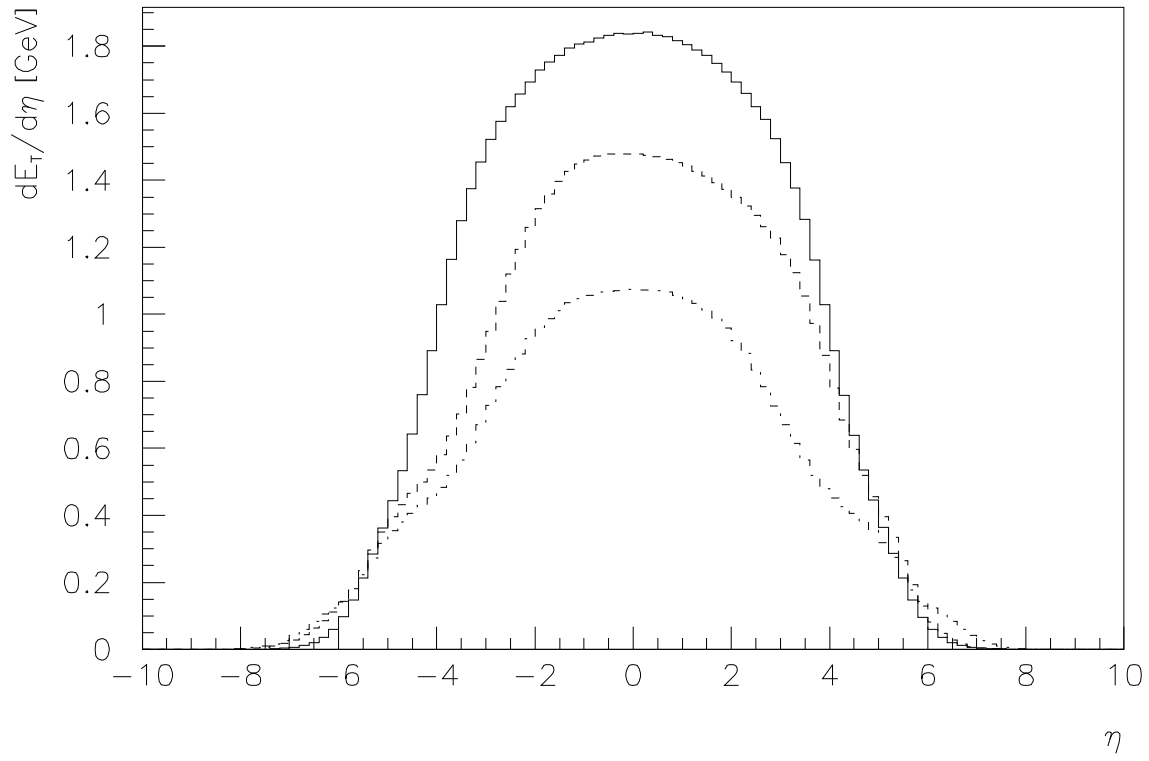

Figure 14: Transverse energy flow as a function of pseudorapidity for different beams. Notation as in Fig. 13.

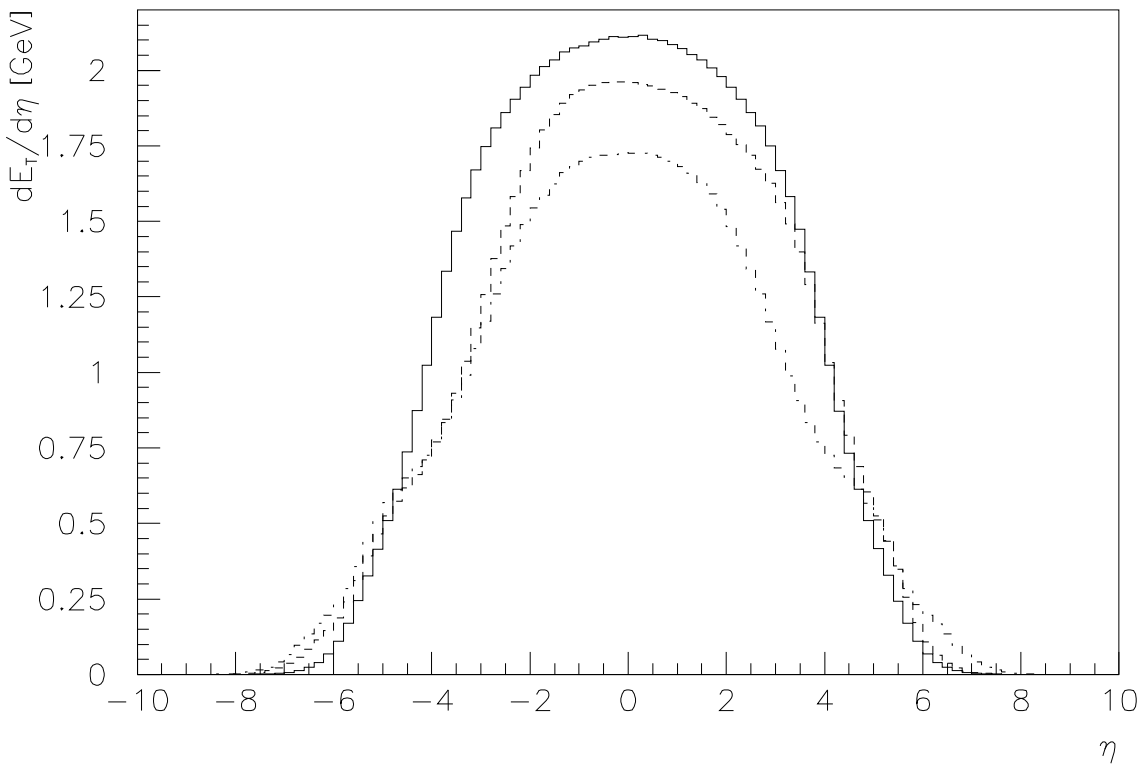

Figure 15: Transverse energy flow as a function of pseudorapidity for different beams, as in Fig. 14 except that elastic and single diffractive events have been removed. Notation as in Fig. 13.

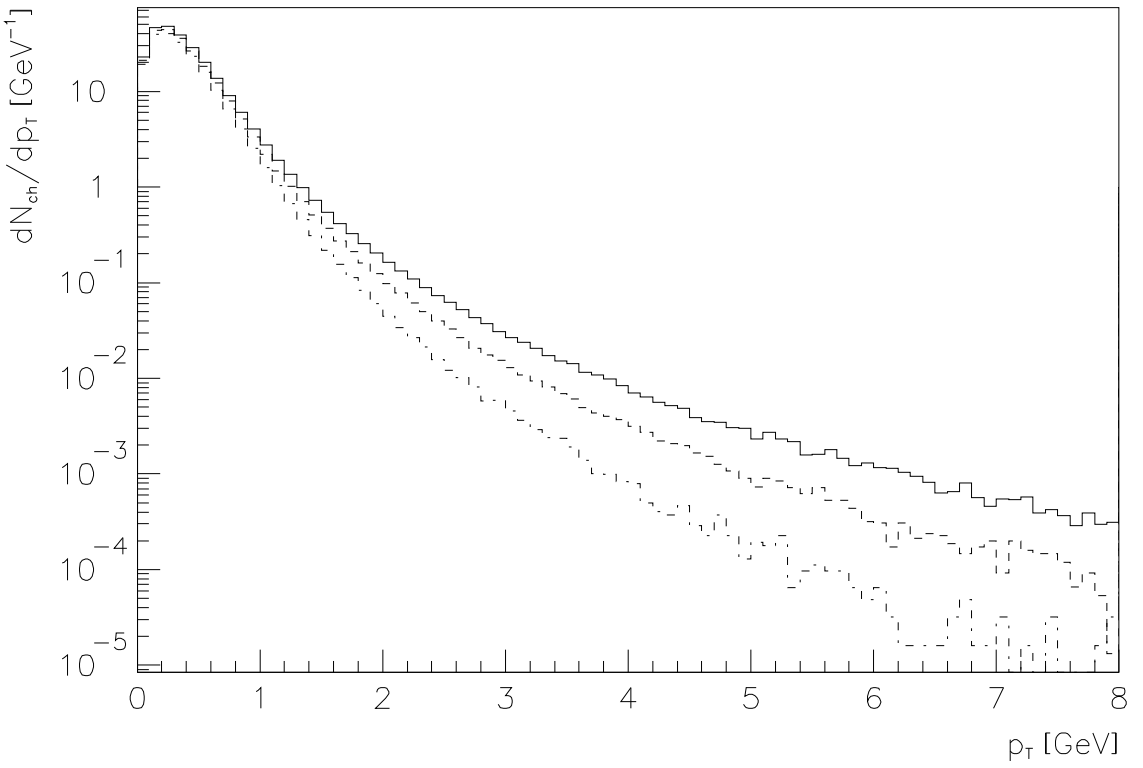

Figure 16: Charged particle inclusive $p_\perp$ spectra for different beams. Notation as in Fig. 13.

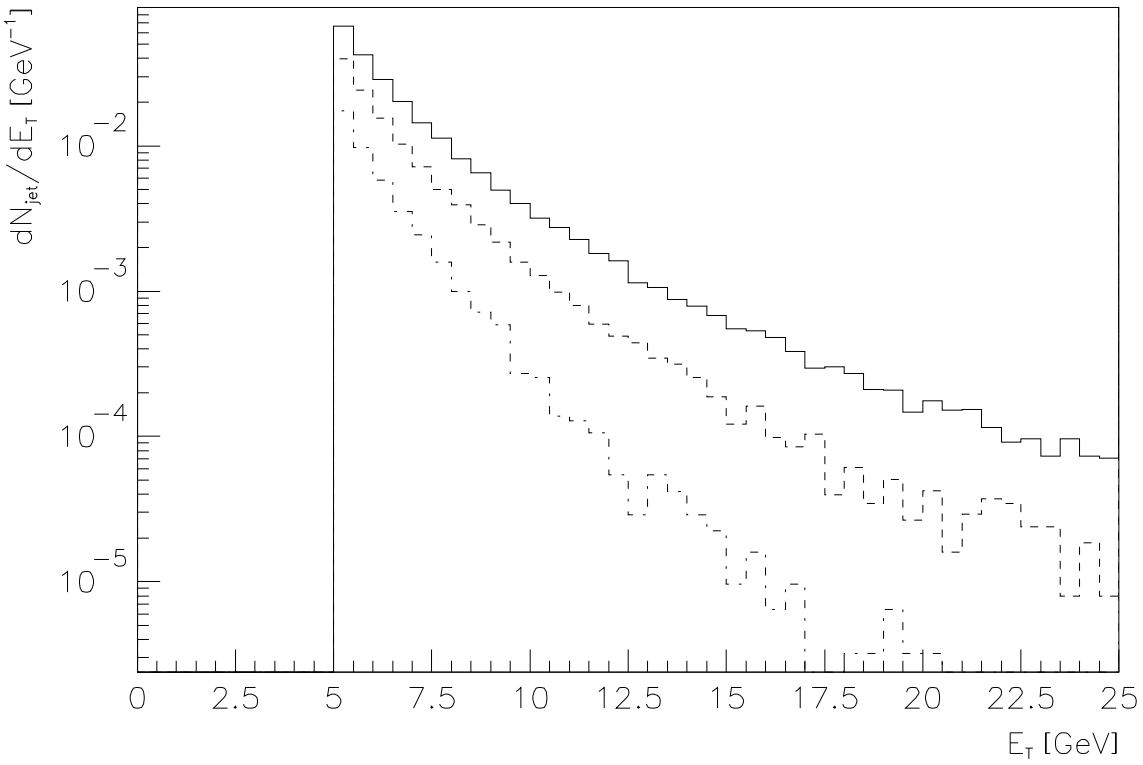

Figure 17: Rate of reconstructed jets as a function of the transverse jet energy for different beams. Notation as in Fig. 13.

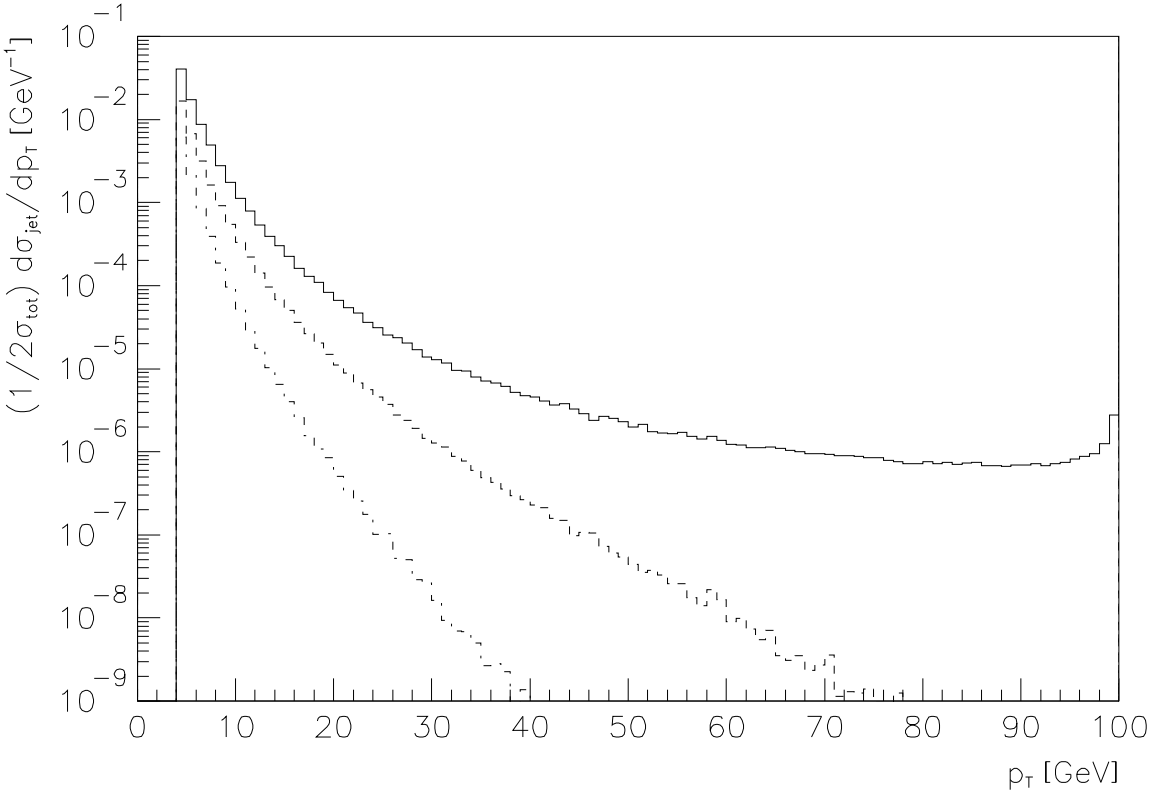

Figure 18: Parton-level jet $p_\perp$ distributions for different beams. The factor 1/2 compensates for there being 2 jets per event. Notation as in Fig. 13.

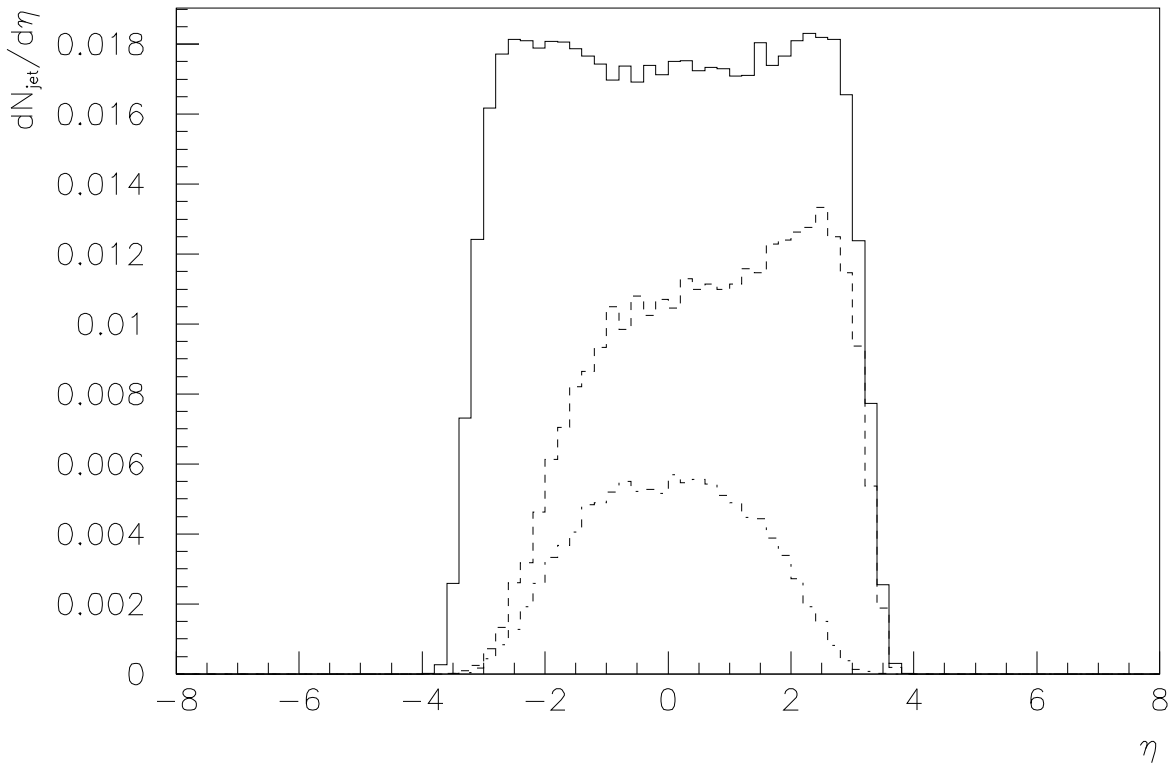

Figure 19: Pseudorapidity distribution of reconstructed jets for different beams. Notation as in Fig. 13.

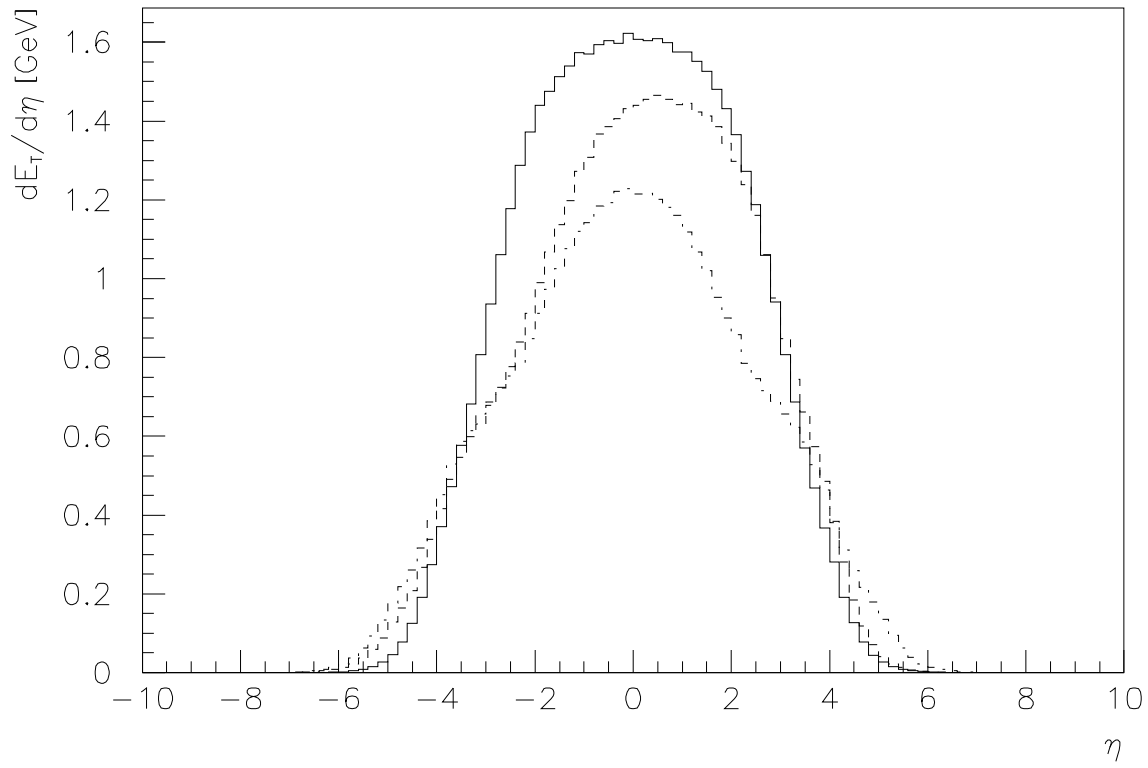

Figure 20: Transverse energy flow for $E_{\rm cm} = 50$ GeV as a function of pseudorapidity for different beams, cf. Fig. 15. Notation as in Fig. 13.